INDC(NDS)-0742
Distr. IN, G

IAEA
International Atomic Energy Agency

INDC International Nuclear Data Committee

Analysis of the U-238 Livermore Pulsed Sphere Experiments Benchmark Evaluations

Prepared by

Tanja Goričanec
Jožef Stefan Institute, Ljubljana, Slovenia

Andrej Trkov
IAEA, Vienna, Austria

Roberto Capote Noy
IAEA, Vienna, Austria

November 2017

IAEA Nuclear Data Section
Vienna International Centre, P.O. Box 100, 1400 Vienna, Austria

Selected INDC documents may be downloaded in electronic form from
http://www-nds.iaea.org/publications
or sent as an e-mail attachment.
Requests for hardcopy or e-mail transmittal should be directed to
NDS.Contact-Point@iaea.org
or to:
Nuclear Data Section
International Atomic Energy Agency
Vienna International Centre
PO Box 100
1400 Vienna
Austria

Printed by the IAEA in Austria

November 2017

Table of Contents

Analysis of the U-238 Livermore Pulsed Sphere Experiments Benchmark Evaluations

Tanja Goričanec, Andrej Trkov, Roberto Capote Noy

Abstract

Work on the analysis of the ^{238}U Livermore Pulsed Sphere experiments relevant for the validation of the CIELO evaluation is presented. The aim of the work described in this report was to validate the new ENDF/B-VIII.0 nuclear data library by comparing calculations to the benchmark experiments. The pulsed sphere experiments were performed at the Lawrance Livermore National Laboratory (LLNL). Different references describing the experimental configuration were reviewed. The evaluated experiments with their characteristics are listed. Calculations were performed using Stephanie C. Frankle reference benchmark model received from Denise Neudecker (LANL). The calculated neutron spectra with a reference model were compared with the experimental values for different experimental configurations and various deviations were observed. Due to the inconsistent results of different detectors the possible reasons for discrepancies (e.g. flight path length, detector angle, etc.) were evaluated. It was concluded that the uncertainty in the flight path length and detector angle have negligible effect on the detected neutron spectra, however the effect of not explicitly modelling experimental geometry can not be neglected. To evaluate the bias due to the not explicitly modelled experimental geometry a detailed computational model with Monte Carlo neutron transport code MCNP was made. In addition, it was found out that the neutron source included in the MCNP model does not take into account the additional neutron peak at ∼2.8 MeV and the calculated results are considered to be less reliable below ∼4 MeV.

1 Introduction

The purpose of the consultancy was to work on the analysis of the U-238 Livermore Pulsed Sphere experiments relevant for the validation of the CIELO evaluations. The pulsed sphere experiments were carried out at the Lawrence Livermore National Laboratory (LLNL) between the 1960 and 1985. The aim of the experiments was to measure 14-MeV neutron leakage spectra from the target spheres made out of various elements, compounds and mixtures. Data from these experiments have been and continue to be fundamental in the evaluation of the neutron Monte Carlo transport codes and cross section data libraries. Therefore, it was considered important to validate the new ENDF/B-VIII.0 nuclear data library with the pulsed sphere benchmark experiments. The primary purpose of this benchmark experiments was to address the need for detailed neutron transport measurements that were sufficiently simple to calculate, yet complex enough to test some of the more sophisticated features of the transport codes and cross-section data. The neutron emission spectrum was measured using time-of-flight techniques over an energy range from 10 eV to 14 MeV. Between 10 eV and 1 MeV (low energy spectra) a ^{6}Li loaded glass scintillator was used, while between 2 and 15 MeV (high energy spectra) a Pilot B or NE213 scintillators were used. This report focuses on the evaluation of the high energy spectrum. Experiments were performed using two ^{238}U spheres with different diameters:

0.8 mfp and 2.8 mfp. Detectors measuring the time of flight of the neutrons were positioned in different beamlines forming 26°, 38.8877° and 116.7053° with the incident deuteron beamline. In the concrete walls surrounding the sphere, the holes were drilled and neutron detectors were positioned behind them. To eliminate the contribution of the scattered neutrons in the air or surrounding structures to the detector signal, the collimator was positioned inside the hole in the wall. The pulsed sphere problem is also very interesting from physics point of view and some interesting phenomena when simulating the problem are described in reference [1].

2 Experimental configuration

The pulsed sphere experiments were performed at the now-decommissioned ICT (Insulated Core Transformer) accelerator at the LLNL. The spheres had a conical openings to allow the neutron source to be centered in the sphere. Neutrons at a nominal energy of 14 MeV were generated via ^{3}H(d,n)^{4}He reaction by a 400 keV deuteron beam impinging on a tritiated titanium target. Over the time many experiments were repeated and some of them were improved, therefore description of the experimental configuration from different references is reported according to the report date.

Reference [2] was very rich in information of the experimental configuration. Reference [2] describes the Livermore ICT facility as: *"400-keV D^{+} ions are accelerated by the Livermore ICT (Insulated Core Transformer) accelerator and impinge upon a tritium-loaded titanium target located approximately at the center of a cubical 40-ft target pit. The target pit incorporates a low-mass aluminum floor to minimize the scattering of the primary neutrons; holes were drilled into the target pit walls in order to accomodate collimators that shield the detectors from the target pit background. The facility has the capability of providing a pulsed neutron source sufficiently variable in pulse width, frequency, and intensity to be ideally suited to a wide range of experiments."*. It also states that the neutron yield was determined using a solid-state alpha detector. Figure 1 shows a schematic drawing of a low-mass target assembly from reference [2]. It also included some additional description of a target assembly: *"The tritium-titanium target backing is a tungsten disk 2.06 cm in diameter by 0.051 cm thick. The evaporated titanium thickness is approximately 4 mg/cm^{2}, and the volume of the absorbed tritium is approximately 3 cm^{3} at STP"*.

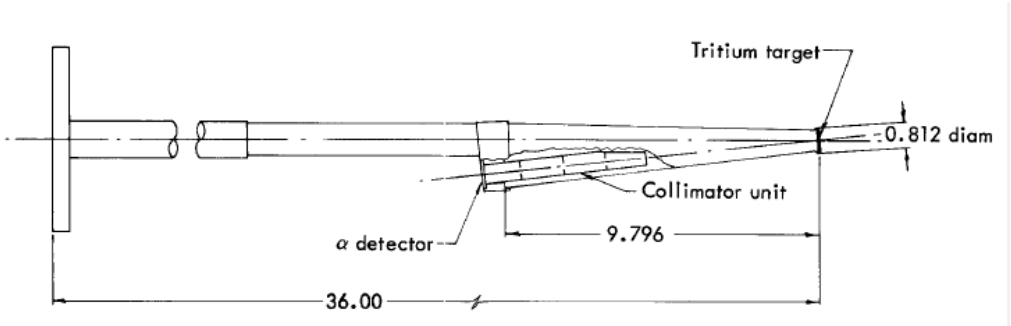

Figure 1: Schematic drawing of the tritium target low-mass assembly. Indicated dimensions are in inches [2].

In reference [2] information about the dimensions and material composition of collimator inside the wall (Figure 2), target assembly (Figure 3) and detector (Figure 4) was found. Reference gives the description of the collimator as: *"The collimator face was aligned with the target pit wall. The collimator was constructed from iron and borated paraffin and was placed in a 31-cm-diam hole in the target pit wall. Three sets of collimator inserts were built to accommodate the entire range of sphere*

sizes. The criterion used was that with the particular collimator set, the detector should view the entire sphere. The collimator shown in Figure 2 is the one used with the intermediate spheres. The high-energy pulsed sphere measurements utilized holes at 30° and 120° with the appropriate collimator assembly. Some of the low-energy measurements were carried out at 26° with respect to the deuteron beam line. Here the collimation was a 20-cm hole in the 2-m thick concrete pit wall. The detector was supported by strings in the center of a large enclosure in order to minimize counts due to outscattering of the primary flux (mainly 14-MeV) by the detector assembly and subsequent inscattering at later times due to materials surrounding the detector. ".

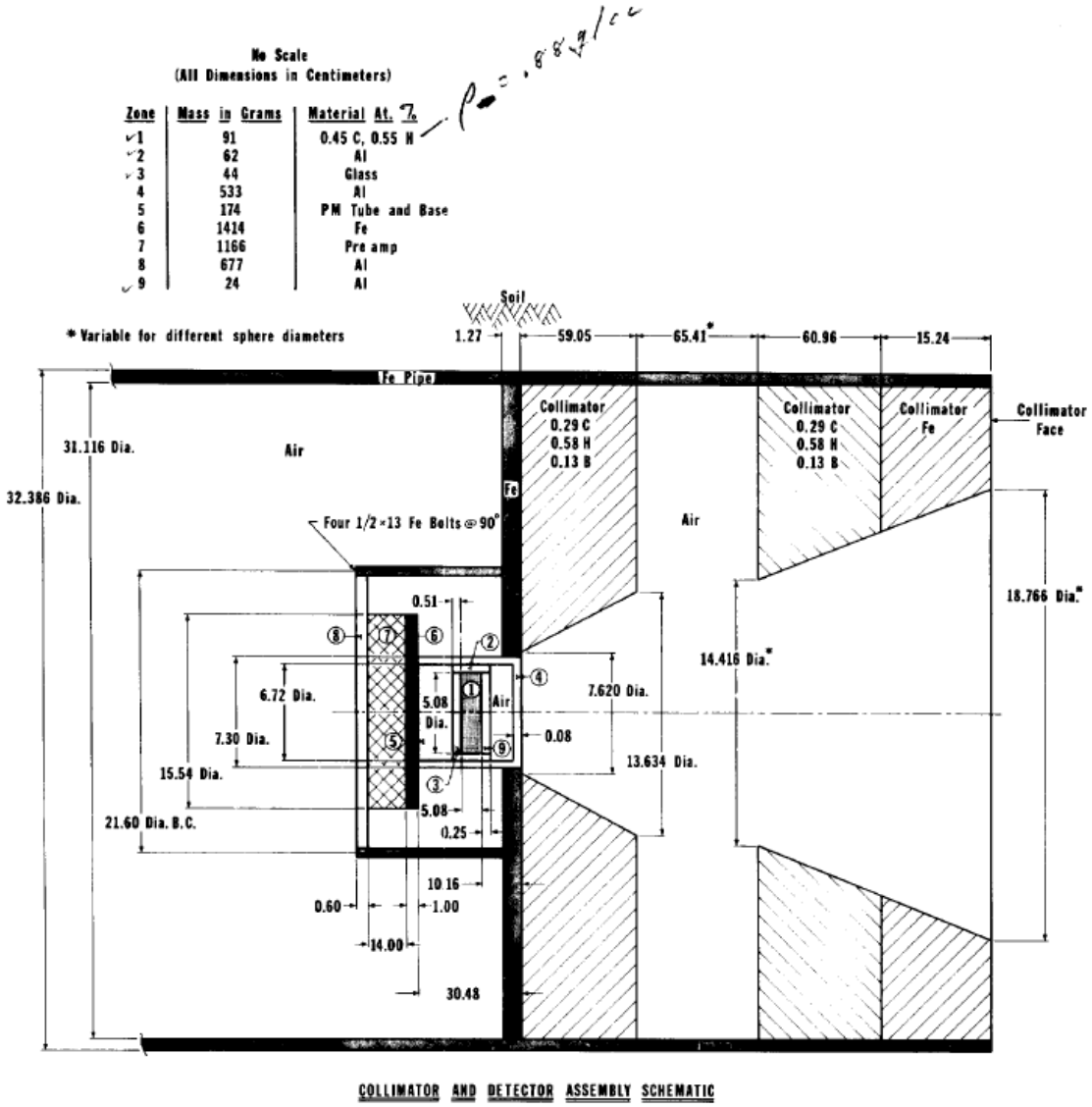

Figure 2: Technical drawing of the collimator and detector geometry [2].

Reference [2] also describes the characteristics of the T(d,n)^{4}He neutron source and its angular and energy distribution. It states: *"The T(d,n)^{4}He reaction below 400-keV deuteron energy is isotropic in the center-of-mass system. The anisotropy in the source neutrons arises from the center-of-mass to laboratory transformation and from 90° edge absorption in the tungsten disk."* The most probable reaction energy for 400-keV bombarding on the ICT was 200 keV. Reference [2] also describes in more detail the determination of angular energy distribution and the relative and absolute source strength determination.

In reference [2] the description of the Pilot B and NE213 detector package was reported: *"The location of the detector package with respect to the collimator assembly is shown in Figure 2. The 5.08-cm diam × 5.08-cm-long liquid scintillator (NE213) is encased in an aluminium can which is sealed with a 0.51-cm-thick glass plate. The 5.08-cm-diam × 5.08-cm-long Pilot B scintillator is coupled to a 8575 RCA photomultiplier tube with a 2.54-cm-long lucite pipe. The scintillator and light pipe are covered with aluminium foil, and this assembly - including the photomultiplier tube - is then covered with black electrical tape".* The detector package is shown in Figure 4. The construction of the NE213 scintillator is also shown in Figure 2. Reference [2] also describes the determination of the efficiency of Pilot B and NE213 as a function of neutron energy in more detail.

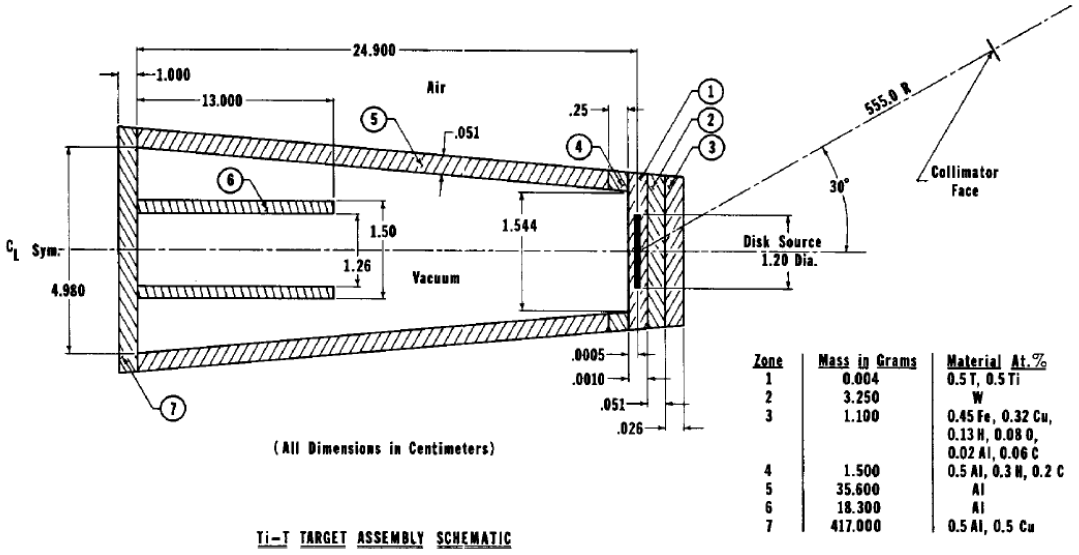

Figure 3: Technical drawing of idealized target assembly [2].

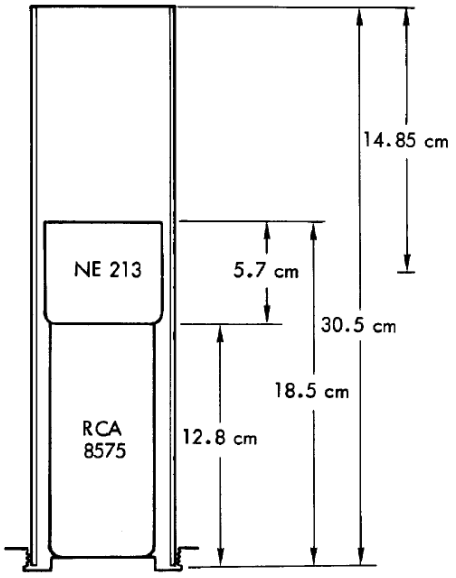

Figure 4: Schematic drawing of the detector package for the high energy emission spectra measurements [2].

Reference [3] describes early calculational models for LLL pulsed spheres together with a discussion of the effects of simplifications. Data relevant to detector response functions, geometric configurations, and other information required in order to calculate time spectra of detected neutrons are included. This reference also describes the experimental method: *"The experiment consists of recording the ratio of counts with the sphere material in to counts with the sphere material out. With this differencing technique, the effects of the low-mass target assembly, the detector collimator, and the air in the flight path between the target and the detector assembly cancel out, and hence have no significant effect on the experimental data. In particular, with the sphere out, the counting rate from neutrons which are scattered from the target assembly and collimator is three orders of magnitude less than the counting rate from the uncollided beam. Therefore, only the portions of the sphere-in neutron spectrum that have three-order-of-magnitude peak-to-valley changes in the counting rate will be affected. The largest effects are for the strongly-forward-peaked heavy elements - Pt,* ^{235}U, ^{238}U *and* ^{239}Pu. *The (nominal) 14 MeV neutron source pulse from the ICT deuteron accelerator has a time behaviour that is nearly Gaussian in shape, with the time spread in the source characterized by its full width at half maximum (FWHM). The detectors were placed at two angles, 30° and 120°, with respect to the incident deuteron beam, and the NE213 and Pilot-B scintillators were 5.08 cm in diameter and 5.08 cm long."*. The information about the experimental configuration presented in this reference agrees with information from other references. In reference the neutron energy-dependent response functions for Pilot-B and NE213 are given and are reproduced as Figure 5 and 6. For the NE213 detector the neutron energy dependent response function was also reported in reference [5] and is presented in Figure 9.

E(MeV)	AE	E(MeV)	AE	E(MeV)	AE
1.600	0.001	6.600	4.791	11.600	3.733
1.700	0.669	6.700	4.747	11.700	3.716
1.800	1.239	6.800	4.720	11.800	3.700
1.900	1.727	6.900	4.684	11.900	3.685
2.000	2.151	7.000	4.641	12.000	3.670
2.100	2.515	7.100	4.615	12.100	3.657
2.200	2.833	7.200	4.568	12.200	3.643
2.300	3.108	7.300	4.479	12.300	3.630
2.400	3.349	7.400	4.429	12.400	3.618
2.500	3.558	7.500	4.400	12.500	3.608
2.600	3.726	7.600	4.362	12.600	3.598
2.700	3.887	7.700	4.340	12.700	3.588
2.800	4.010	7.800	4.325	12.800	3.580
2.900	4.088	7.900	4.320	12.900	3.573
3.000	4.242	8.000	4.309	13.000	3.565
3.100	4.366	8.100	4.313	13.100	3.560
3.200	4.408	8.200	4.317	13.200	3.557
3.300	4.446	8.300	4.316	13.300	3.556
3.400	4.483	8.400	4.314	13.400	3.556
3.500	4.527	8.500	4.304	13.500	3.557
3.600	4.572	8.600	4.296	13.600	3.560
3.700	4.615	8.700	4.287	13.700	3.571
3.800	4.660	8.800	4.278	13.800	3.583
3.900	4.707	8.900	4.260	13.900	3.600
4.000	4.774	9.000	4.243	14.000	3.613
4.100	4.765	9.100	4.216	14.100	3.625
4.200	4.766	9.200	4.189	14.200	3.638
4.300	4.761	9.300	4.171	14.300	3.651
4.400	4.786	9.400	4.153	14.400	3.664
4.500	4.807	9.500	4.136	14.500	3.677
4.600	4.824	9.600	4.120	14.600	3.690
4.700	4.832	9.700	4.103	14.700	3.703
4.800	4.835	9.800	4.086	14.800	3.716
4.900	4.839	9.900	4.066	14.900	3.729
5.000	4.845	10.000	4.045	15.000	3.741
5.100	4.846	10.100	4.030	15.100	3.753
5.200	4.847	10.200	4.006	15.200	3.765
5.300	4.845	10.300	3.985	15.300	3.777
5.400	4.840	10.400	3.960	15.400	3.789
5.500	4.836	10.500	3.943	15.500	3.801
5.600	4.833	10.600	3.920	15.600	3.813
5.700	4.833	10.700	3.900	15.700	3.825
5.800	4.836	10.800	3.880	15.800	3.837
5.900	4.840	10.900	3.860	15.900	3.849
6.000	4.842	11.000	3.840	16.000	3.861
6.100	4.844	11.100	3.820		
6.200	4.840	11.200	3.800		
6.300	4.832	11.300	3.783		
6.400	4.820	11.400	3.766		
6.500	4.805	11.500	3.750		

Figure 5: Pilot-B detector response function [3].

E(MeV)	AE	E(MeV)	AE	E(MeV)	AE
1.600	0.003	6.600	4.155	11.600	3.116
1.700	0.615	6.700	4.126	11.700	3.101
1.800	1.139	6.800	4.107	11.800	3.088
1.900	1.586	6.900	4.091	11.900	3.074
2.000	1.974	7.000	4.069	12.000	3.062
2.100	2.306	7.100	4.050	12.100	3.050
2.200	2.596	7.200	4.020	12.200	3.040
2.300	2.846	7.300	3.954	12.300	3.031
2.400	3.065	7.400	3.918	12.400	3.022
2.500	3.255	7.500	3.898	12.500	3.013
2.600	3.417	7.600	3.882	12.600	3.006
2.700	3.555	7.700	3.830	12.700	2.998
2.800	3.668	7.800	3.814	12.800	2.992
2.900	3.744	7.900	3.805	12.900	2.988
3.000	3.876	8.000	3.787	13.000	2.984
3.100	3.984	8.100	3.767	13.100	2.982
3.200	4.027	8.200	3.771	13.200	2.981
3.300	4.064	8.300	3.761	13.300	2.980
3.400	4.100	8.400	3.744	13.400	2.980
3.500	4.140	8.500	3.727	13.500	2.981
3.600	4.180	8.600	3.704	13.600	2.982
3.700	4.217	8.700	3.684	13.700	2.987
3.800	4.255	8.800	3.663	13.800	2.992
3.900	4.294	8.900	3.641	13.900	2.998
4.000	4.325	9.000	3.618	14.000	3.004
4.100	4.342	9.100	3.588	14.100	3.010
4.200	4.344	9.200	3.562	14.200	3.016
4.300	4.340	9.300	3.542	14.300	3.021
4.400	4.359	9.400	3.525	14.400	3.027
4.500	4.375	9.500	3.506	14.500	3.032
4.600	4.388	9.600	3.486	14.600	3.038
4.700	4.392	9.700	3.468	14.700	3.043
4.800	4.392	9.800	3.450	14.800	3.049
4.900	4.389	9.900	3.429	14.900	3.055
5.000	4.386	10.000	3.410	15.000	3.061
5.100	4.379	10.100	3.393	15.100	3.067
5.200	4.371	10.200	3.375	15.200	3.073
5.300	4.362	10.300	3.355	15.300	3.078
5.400	4.333	10.400	3.333	15.400	3.083
5.500	4.332	10.500	3.312	15.500	3.087
5.600	4.318	10.600	3.293	15.600	3.092
5.700	4.304	10.700	3.275	15.700	3.097
5.800	4.286	10.800	3.255	15.800	3.102
5.900	4.269	10.900	3.238	15.900	3.106
6.000	4.250	11.000	3.217	16.000	3.110
6.100	4.228	11.100	3.200		
6.200	4.199	11.200	3.180		
6.300	4.102	11.300	3.162		
6.400	4.167	11.400	3.148		
6.500	4.155	11.500	3.130		

Figure 6: NE213 detector response function [3].

In reference [4] additional schematic drawing of the experimental configuration was found and is reproduced as Figure 7, however it should be noted that reference [4] is describing measurements of lower energy range (between 10 eV and 1 MeV) performed with ^{6}Li loaded glass scintillator and is therefore the least applicable to the evaluation of the experiments presented in this report.

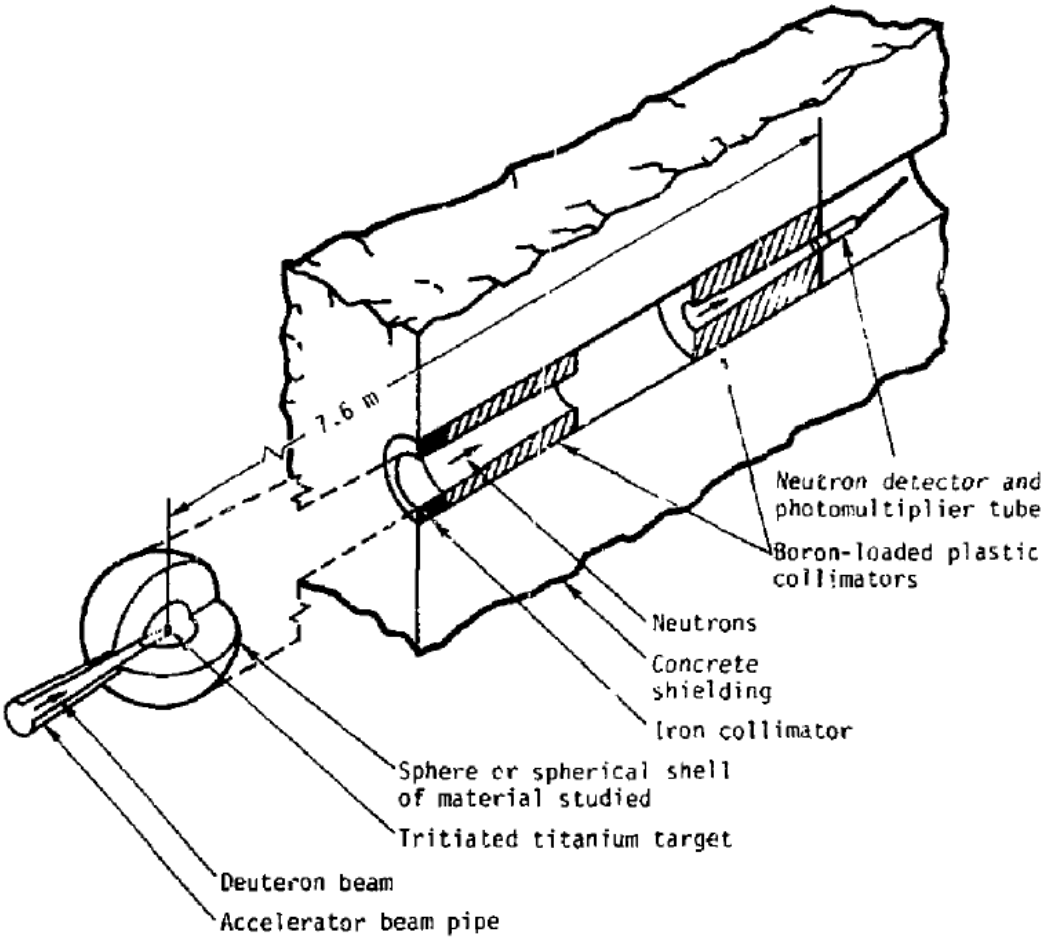

Figure 7: Pulsed sphere geometry [4].

In reference [5] another schematic drawing of the experimental configuration was found and is represented as Figure 8. Reference [5] describes measurements performed with scintillation detectors (NE213) at 26° and 120° with respect to the deuteron beam and at flight paths from 7.5-9.8 m.

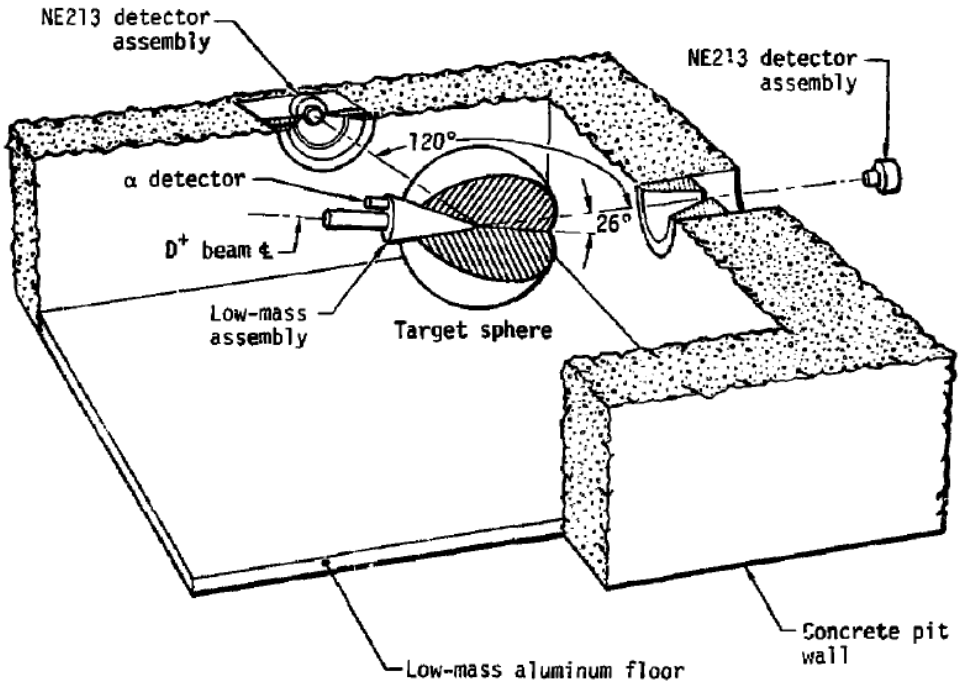

Figure 8: Efficiency of the NE213 scintillation detector [5].

The experimental method is in reference [5] described as: *"Neutrons were produced at the center of the spherical targets by a 400-keV deuteron beam impinging on tritinted titanium that had been deposited on a tungsten disk. The neutron source strength was monitored by a solid state detector measuring the alpha particles associated with the T(d,n)^{4}He reaction. Because we used the target-in/target-out technique, only the relative neutron production had been determined. This value was obtained from the ratio of total neutron counts in the detector to the total number of alpha particles detected during a target-out accelerator run. Thus the relative neutron source strength during the target-in run is the product of the relative neutron production and the integrated alpha count. The neutron detectors were located in collimated ports in the concrete walls of the target room. Our most recent experiments were conducted with NE213 liquid scintillaton detectors. The time-dependent gamma pulse that is produced by inelastic collision in the target was virtually eliminated by pulse-shape discrimination. (For the original pulsed-sphere experiments, we employed a Pilot-B detector without the gamma suppresion feature and, as a result, the strong gamma-ray pulse obscured a significant portion of the time-of-flight spectrum.) In addition, the time-independent gamma background that results from de-excitation gamma rays from neutron capture reactions is considerably reduced with the NE213 detector system. This new detector with the gamma suppression feature plus improved deuteron beam bouncing and sweeping has yield data of considerably quality. For this reason we are repeating many of our early pulsed-sphere experiments"*. The reference describes in detail the calibration method for different experimental configurations. It also states that the detectors were collimated and that the detailed description of the NE213 detectors is presented in reference [2]. The neutron detection efficiencies

at the two detector treshold energies (1.6 and 2.2 MeV) employed in the experiments presented in reference [5] are presented in Figure 9. Detector efficiency is expressed as $A\epsilon$, where A is the cross-sectional area of the detector in square centimeters and ϵ is the detection probability.

Low threshold (1.6 MeV)		High threshold (2.2 MeV)	
E(MeV)	Aε	E(MeV)	Aε
1.8	1.46	2.5	1.00
1.9	1.86	2.6	1.30
2.0	2.26	2.7	1.60
2.1	2.58	2.8	1.85
2.2	3.00	2.9	2.10
2.3	3.29	3.0	2.35
2.4	3.42	3.1	2.55
2.5	3.63	3.2	2.70
2.75	3.95	3.3	2.85
3.0	4.10	3.4	2 95
3.5	4.25	3.5	3.05
4.0	4.33	4.0	3.35
4.5	4.39	4.5	3.57
5.0	4.40	5.0	3.70
5.5	4.37	5.5	3.75
6.0	4.28	6.0	3.75
6.4	4.15	7.0	3.70
6.6	4.20	8.0	3.55
6.8	4.18	9.0	3.40
7.0	4.12	10.0	3.20
7.5	3.97	11.0	3.05
8.1	3.80	12.0	2.90
8.5	3.77	13.0	2.75
9.0	3.65	13.6	2.71
10.0	3.44	14.0	2.67
11.0	3.24	15.0	2.65
12.0	3.06		
12.5	3.01		
13.0	2.98		
13.5	2.98		
14.0	3.01		
15.0	3.08		
16.0	3.25		

Figure 9: The neutron energy dependent response function for NE213 detector [5].

In reference [6] another schematic representation of the experimental configuration was found and is presented in Figure 10. In reference [6] aditional information about experiments was found: *"Pilot-B and NE213 scintillators were used for the 2 to 15 MeV measurements. They were placed at angles of 26°, 30° and 120° with respect to the incident d-beam direction, and they had flight paths ranging from 750 to 975 cm."*. The statement about the detectors angles is in agreement with the experimental drawing in Figure 10, however it dissagrees with the drawing from reference [5] presented in Figure 8, where it seems that the reported angles 30° and 120° were measured with respect to the 26° beam-line and were all in the same axial plane inside the wall. This contradictory information were addressed in the sensitivity analyses.

The measured data for each spherical assembly (target in) was normalized to the total flux measured with the material of interest removed from the spherical assembly (target out) [6].

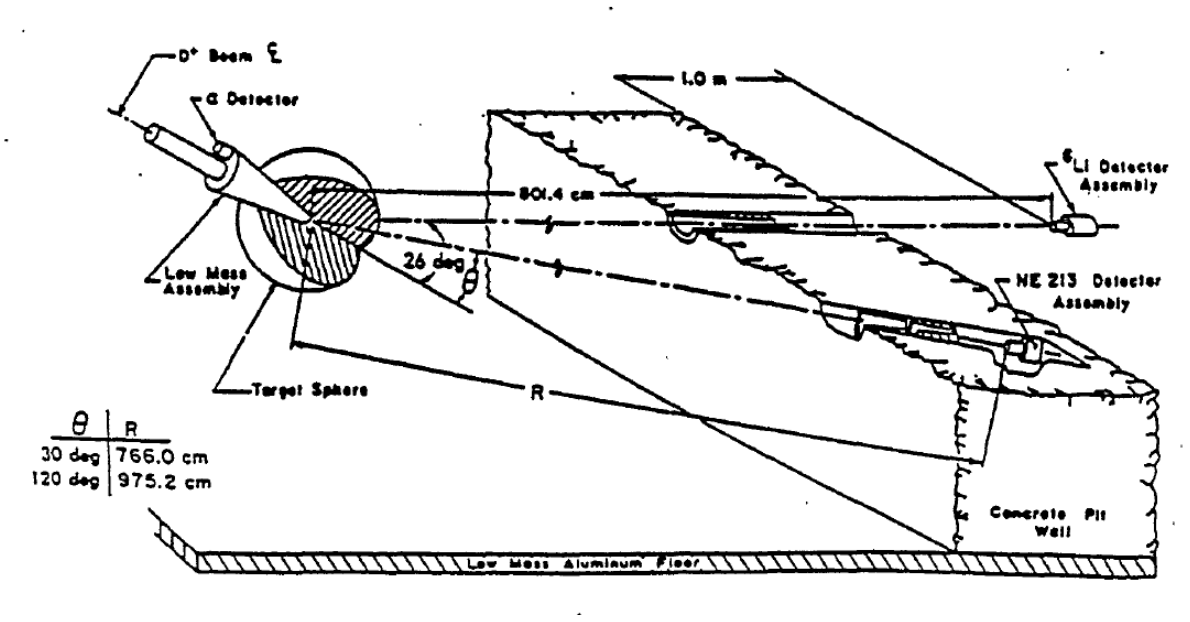

Figure 10: Experimental setup for the LLNL pulsed sphere measurements [6].

The deuteron beam line formed 26° angle with the floor [7]. Schematic drawing of the accelerator, beam transport, target sphere, collimator and detector assembly found in reference [7] is reproduced as Figure 11. In Reference [7] additional information was found: *"The facility consisted of a 12.2 m cubic target pit with ~ 2 m thick concrete walls connected to a separate detector room by a tunnel in which a cylindrical collimator was inserted. The target sphere was located close to a center of the target pit. Mass near the sphere and detector was kept minimum to reduce background scattering."*

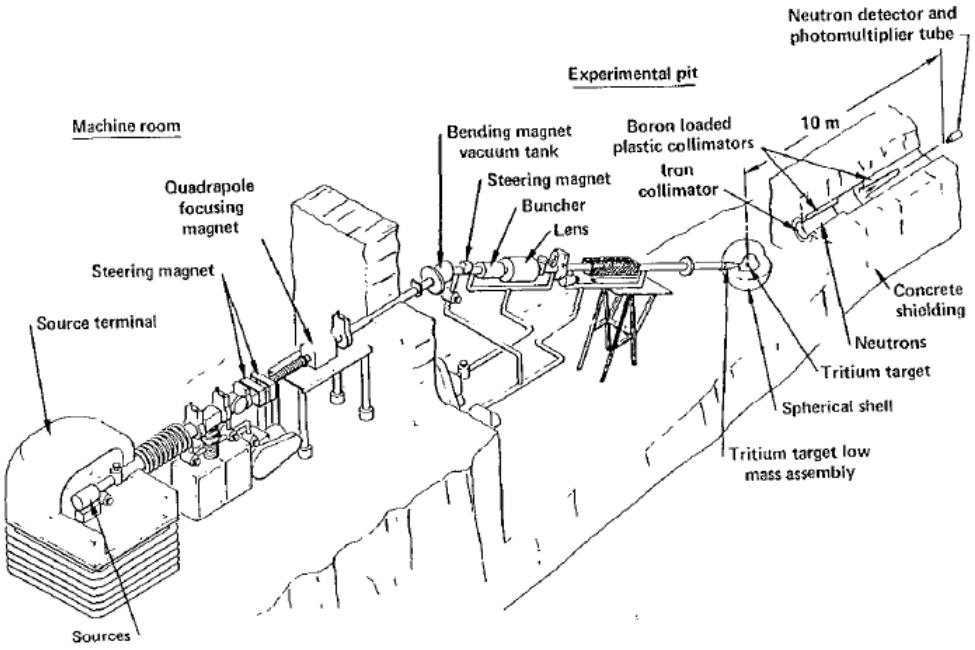

Figure 11: Schematic view of the accelerator, beam transport, target sphere, collimator and detector assembly - not to scale [7].

Reference [8] is a summary of new measurements and calculations for pulsed spheres. It contains a list of all relevant publications and summary table of experiments.

Reference [9] describes the improvements made in the evaluation of the pulsed sphere experiments. They went through the datafiles containing the results of all experiments and extracted the most reliable set of results for each experiment. The second phase of the work was to create an MCNP model for at least one sphere of each material, and to make comparisons of the measured time-dependent spectra) against the spectra calculated using different incident neutron cross section libraries. They confirmed that with Marchetti and Hendstrom's new source specifications results were in much better agreement with the measurements in the high energy range (11 to 15 MeV), and virtually equivalent everywhere else.

Reference [10] is describing evaluation of pulsed sphere experiments using Mercury Monte Carlo neutron transport code. The Mercury model deviates from the other computational models, because it models point detector and not ring detector. In the Mercury model the experimental pit was modelled as 10.24 cubic room surrounded by 2.02 m thick concrete walls. The view of the Mercury computational model is presented in Figure 12.

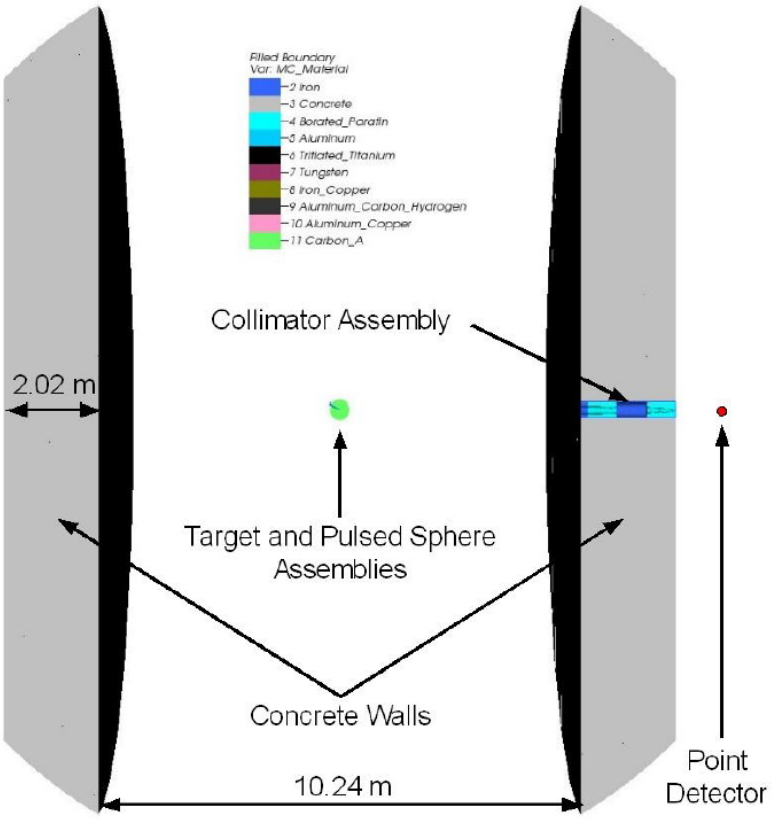

Figure 12: Mercury Monte Carlo computational model of the experimental geometry[10].

3 Evaluated experiments

This report describes evaluation of ^{238}U pulsed sphere experiments. The IAEA has received the most promising experiments and their computational models. It was assumed that the benchmark evaluators already made a well informed choice choosing appropriate experiments. The evaluated experiments are briefly summarized in the Table 3.1. Evaluated were 2 ^{238}U spheres: a smaller one with 3.63 cm (0.8 mfp) radius and larger one with 10.932 cm (2.8 mfp) radius. For smaller sphere, 3 detector positions were evaluated, and, for the larger sphere only 2. Two different subtypes of NE213 detector are marked with letters *a* and *b*. The difference between the subtypes is in the detector response function. According to the Stephanie C. Frankle the experimental configuration 28b is considered the most reliable and should be used for benchmarking.

Table 3.1: Characteristics of evaluated experiments of the ^{238}U pulsed spheres.

Exp. No.	Sphere R [cm]	Detector	Bias [MeV]	Beamline angle [°]	Pulse FWHM [ns]	Flight path [cm]	Reference
08a	3.63	Pilot-B	1.6	30	4.0	765.2	UCID-16372 [3]
08b	3.63	NE213-a	1.6	120	4.0	977.2	UCID-16372 [3]
08c	3.63	NE213-b	1.6	26	2.0	945.54	LAUR-96-2143 [6][(a)]
28a	10.932	Pilot-B	1.6	30	4.0	765.2	Not found
28b	10.932	NE213-b	1.6	26	2.0	746.34	UCRL-131461 [7][(a)]
[(a)] No experimental data presented in table only in graphical form, therefore it was not possible to check the match.							

Experiments reported in reference [5], that were not evaluated are presented in Table 3.2. The reason they were not evaluated is not known, however it is presumed that the experiments were chosen based on well-informed decision.

Table 3.2: Characteristics of experiments of the ^{238}U pulsed spheres that were not evaluated.

Reference	Sphere R [cm]	Detector	Bias [MeV]	Beamline angle [°]	Pulse FWHM [ns]	Flight path [cm]
UCRL-131461 [7]	3.63	NE213-b	0.8	26	2.0	945.54
UCID-17332 [5]	3.63	NE213	1.6	26	4.0	945.3
UCID-17332 [5]	3.63	NE213	1.6	120	3.5	980.1
UCID-17332 [5]	10.932	NE213	1.6	26	4.0	765.3
UCID-17332 [5]	10.932	NE213	1.6	120	3.6	980.1

4 Reference computational model

The basis for the computational evaluation of the experiments were MCNP (Monte Carlo n-particle transport code) inputs, of Stephanie C. Frankle provided by LANL, who send them to the IAEA. In those inputs the experimental geometry is not modelled explicitly, but some simplifications were introduces. Neutron detectors were modelled as ring detectors and not as volume detectors. Also concrete pit walls and collimators inside beamline were not included in the model. However, around the beamline thin layers of concrete were added to simulate the effect of collimators inside the beamline. The neutron importance of those concrete layers was set to 0, which means that they acted as black absorber. The justification of this simplification was also explained in reference [9]. Where they investigated the collimating effect of the wall around the beamline. For the Pu-239 sphere, the collimating effect of the wall around the beamline was found to be negligible. It is stated that: *"Whether the collimating material was concrete or a black absorber made some difference, but not much. Comparison plots show that the effect of neutron reflection back to the sphere from the concrete walls was totally negligible in the timeframe of the measurements. Thus, the black absorber was adopted."* However, in this reference the effect was evaluated for the ^{239}Pu and in case of ^{238}U the effect can be significantly different. Therefore it was decided to evaluate the effect of the concrete or black absorber around beamline in the sensitivity analyses.

The view of the reference model geometry is presented in Figure 13. The simplification in geometry and ring detector geometry can be observed. In Figures 14 and 15, the modelled ^{238}U spheres of different radii can be observed. The incident deuteron beamline in a cone shape entering the sphere can also be observed. In the reference model the coordinate system was positioned in line with a incident deuteron beamline.

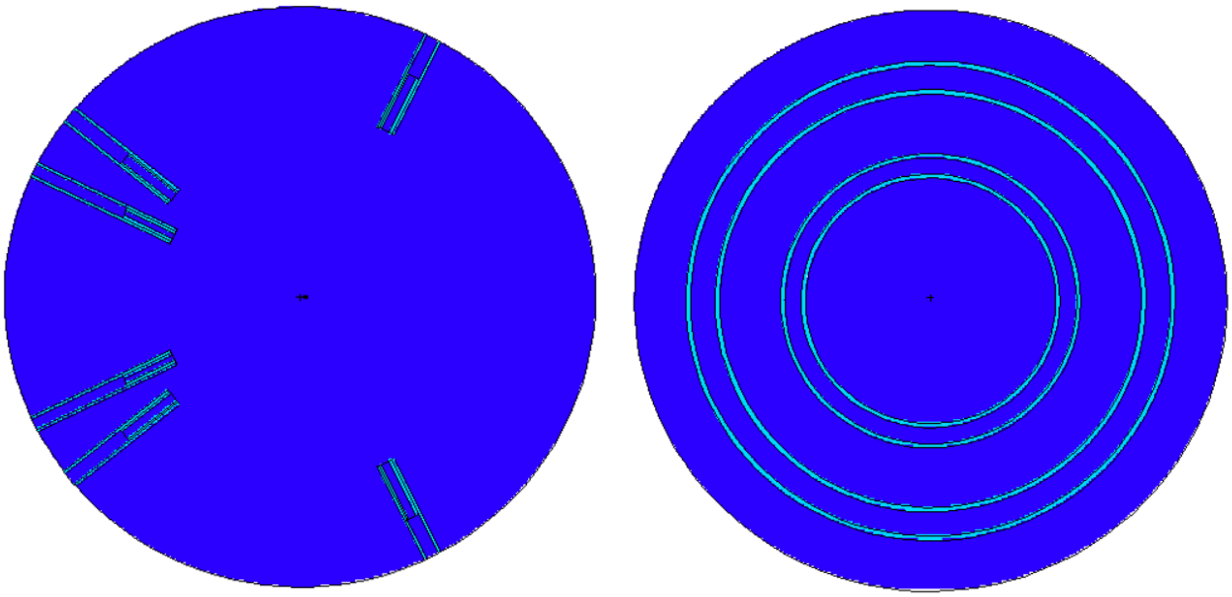

Figure 13: View of the MCNP computational model geometry in the xz-plane (left) and yz-plane (right) view. Dark blue color represents air and light blue color concrete layer around beamlines.

From the schematic drawings of the experimental configuration it was deduced that the incident deuteron beamline had a 26° angle forming with the floor. Therefore detector positioned at 26° angle in regard to the incident deuteron beamline had a beamline going perpendicular to the wall and straight through. From the schematic drawings of the experiment it was also concluded that

the angles 30° and 120° were measured with reference to the 26° beamline and not to the incident deuteron beamline. Considering this the angle between other two beamlines and incident deuteron beamline were calculated to be 38.8877° and 116.7053°, this was already taken into account in the reference model.

The cone representing the incident deuteron beamline and the tritium target were modelled according to the technical drawigs from reference [2], which are presented in Figures 2 and 3.

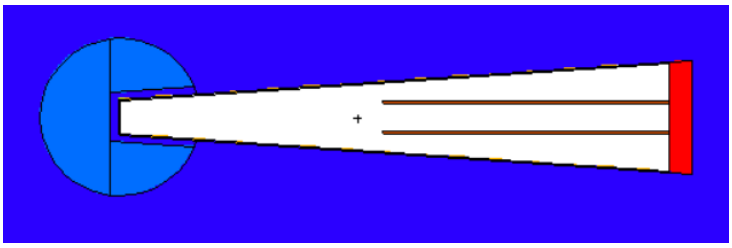

Figure 14: View of the small (0.8 mfp) ^{238}U sphere with incident deuteron beamline in the MCNP model.

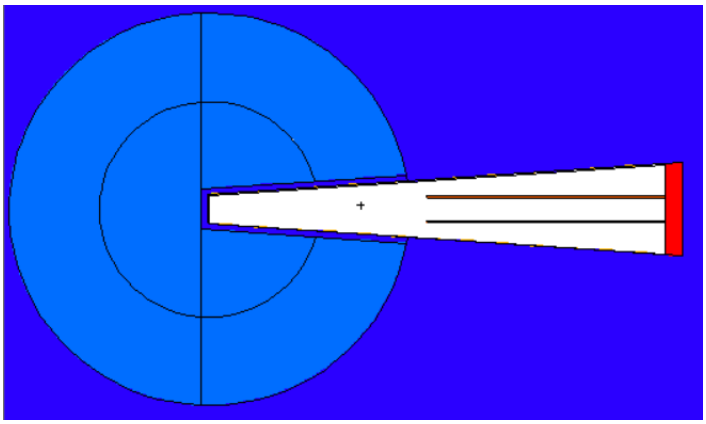

Figure 15: View of the large (2.8 mfp) ^{238}U sphere with incident deuteron beamline in the MCNP model.

In the calculation of neutron spectra, the time of arrival is used in conjunction with a detector response function to make a correction for detector efficiency and thus obtain the true experimental counting rate as a function of time. The efficiency of the detector is given as the product of the detector area A and the probability-of-detection ϵ. The Pilot-B detector neutron energy-dependent response function used in the MCNP model was confirmed to be the same as reported in the reference [3] and presented in Figure 5 with the normalization to the 15 MeV value. Also for the NE213-a detector the neutron energy-dependent response function was used from the reference [3] presented in Figure 6. However, for the NE213-b detector the response function from reference [5] presented in Figure 9. The analysis of the detector response functions is presented in Reference [12], from where the correct response functions used in the reference model were determined.

The transport of the charged particled (deuterons) was not included in the MCNP model, but the neutron source originating from the ^{3}H(d,n)^{4}He reaction was simulated. The neutron source used in the reference benchmark model was new Marchetti's source, which is described in reference [7]. The neutron source spectrum described in reference [7] was not measured, but was calculated. The energy distribution around 14 MeV is angularly distributed as shown in Figure 16. Figure 17 shows

the angular energy spectrum of the neutron source in reference benchmark MCNP model. Neutron pulses produced from the deuteron pulses were modelled using MCNP shakes, taking into account 1 shake is equal to 10^{-8} s. For example, 2 ns pulse was modelled Gaussian distributed with the FWHM=0.2 shake.

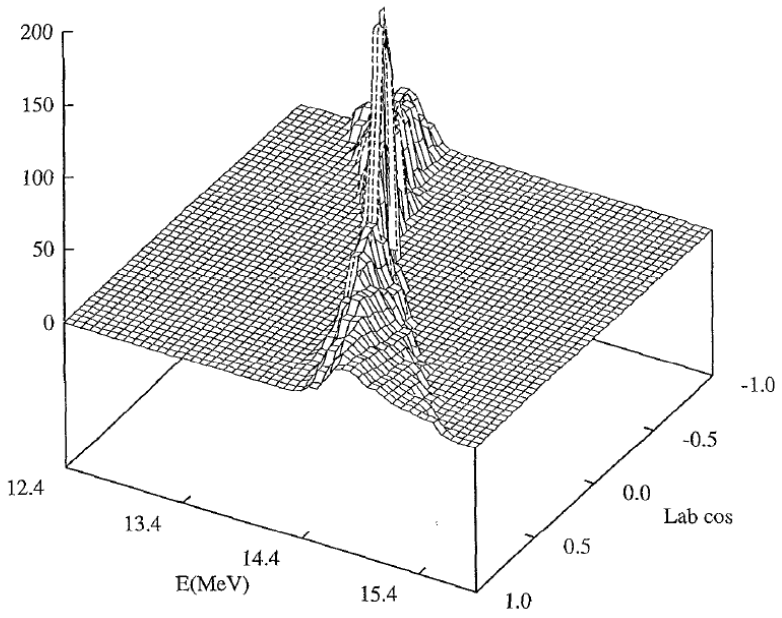

Figure 16: Surface plot of the calculated neutron spectrum as a function of energy and laboratory cosine for the reaction ^{3}H(d,n)^{4}He at 400 keV in a thick titanium target [7].

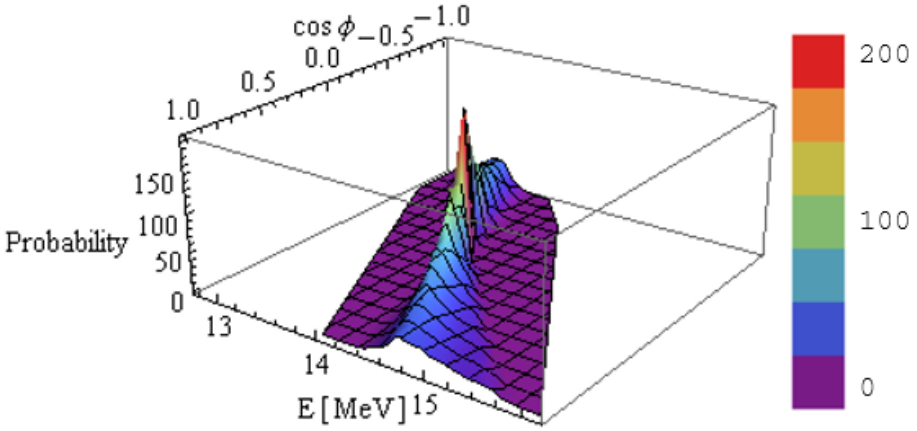

Figure 17: Surfce plot of an angular distribution of the neutron source energy used in the reference benchmark MCNP model.

5 Results and Sensitivity Study

The reference benchmark model was used for comparing calculations with measurements. Calculations were performed using the Monte Carlo neutron transport code MCNP6 [11] with the ENDF/B-VIII.0 data library. The aim of this comparison is to evaluate the new version of the ENDF/B incident neutron cross section library through comparison to the benchmark experiments. The effect of the uncertainties in different parameters on the benchmark result was evaluated. Sensitivity of the calculated neutron spectra to the flight path length, detector angle and concrete layer surrounding the beamline was evaluated.

5.1 Comparison of measurements and calculations

Calculated energy spectrum with the reference computational benchmark model was compared to the measured spectrum for all sphere and detector configurations. Calculations using reference benchmark model were performed using different incident neutron cross section libraries: ENDF/B-VII.1 and two versions of the new evaluation ENDF/B-VIII.0. The evaluated new versions of ENDF data library were ENDF/B-VIII.0 $\beta 4$ (marked as e80b4 in figures) and ENDF/B-VIII.0 $\beta 4+$ (marked as e80b4h2 in figures). The difference between the versions is in the fission spectrum of prompt neutrons above 8 MeV, which is in case of $\beta 4+$ version taken from the JENDL evaluation. Comparison of calculations with different data libraries are presented in Figures 18, 20, 21 and 25. It can be observed that for different experimental configurations the discrepancies between different data libraries change. Therefore, it is hard to conclude which nuclear data library describes the experiments better. For example, the ENDF/B-VII.1 does not describe the experiment 08a and 08b well in the region around 10 MeV, while other data libraries give better agreement. However, in case of the 08c experimental configuration the ENDF/B-VII.1 library gives the best results. In Figure 25, different nuclear data libraries are compared in case of 28b experimental configuration. This experimental configuration was considered to be the most reliable. It can be observed that the new $\beta 4+$ version describes the experiments better than the previous versions. However, the deviations around the minimum are still noticeable. Comparison of results performed with detectors at different angles and at different pulse lengths are presented in Figures 19 and 24. Figure 22 shows the comparison of the measured and calculated time-of-flight spectrum from which the energy spectrum can be calculated as presented in Figure 23. It should be noted that the calculations were performed for the time-of-flight and were than approximately converted to the energy scale by keeping the values on the ordinate axis symmetric and only the abscissa axis was changed according to the flight path length. In case of a detector positioned in 30° beamline (08a, 28a) the discrepancies between the measurements and calculations are higher in the region between 2 and 7 MeV, where a constant deviation in the slope can be observed. Therefore, the sensitivity analyses to the detector flight path and angle were studied and the results are reported in Sections 5.2 and 5.3.

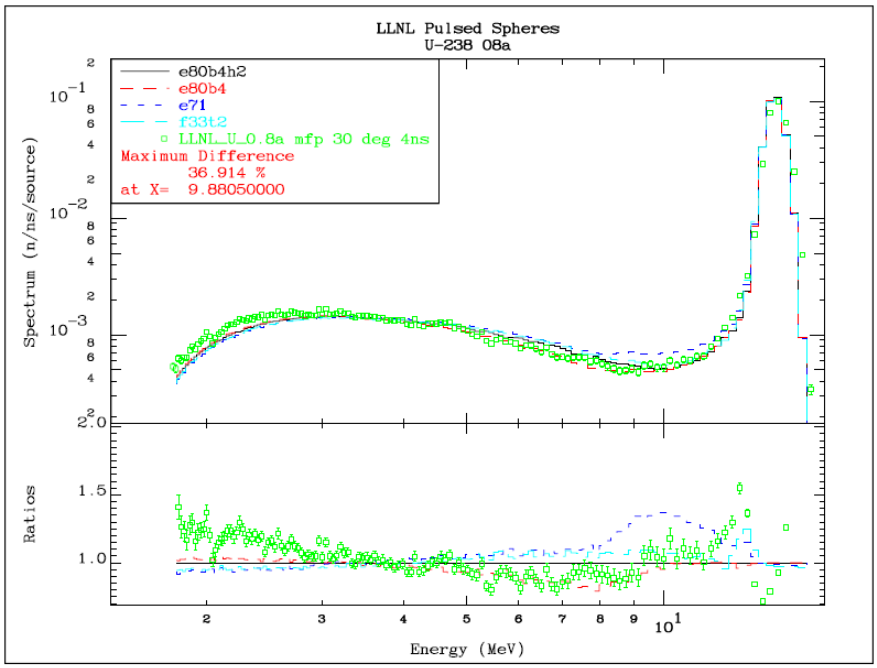

Figure 18: Comparison of neutron spectrum measurements to reference benchmark model calculations for experimental configuration 08a. Measurements are marked with green, reference calculations performed with ENDF/B-VIII.0 β4+ data library are marked with black color (e80b4h2), calculations performed with a previous version of ENDF/B-VIII.0 β4 are marked with red (e80b4) and ENDF/B-VII.1 with blue (e71).

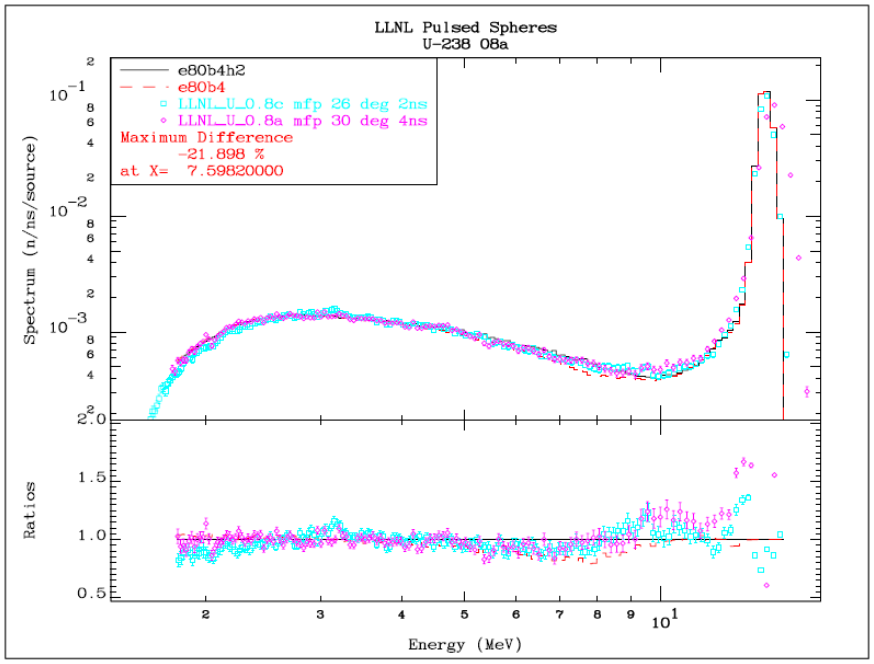

Figure 19: Comparison of neutron spectrum measurements with neutron detectors at different angles to reference benchmark model calculations for experimental configuration 08a. Measurements are marked with light blue (26°) and magenta (30°) and reference calculations for the 26° detector with black and red color.

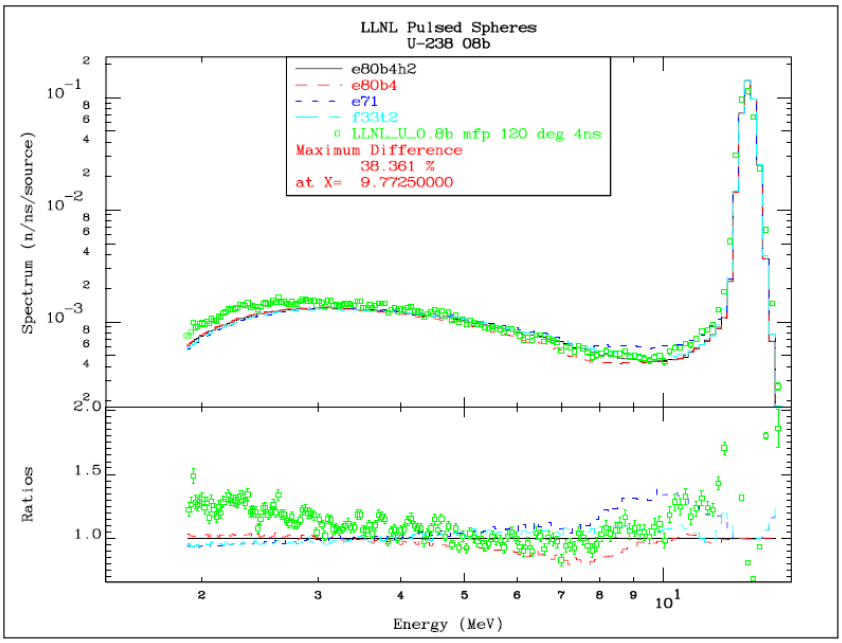

Figure 20: Comparison of neutron spectrum measurements to reference benchmark model calculations for experimental configuration 08b. Measurements are marked with green, reference calculations performed with ENDF/B-VIII.0 β4+ data library are marked with black color (e80b4h2), calculations performed with a previous version of ENDF/B-VIII.0 β4 are marked with red (e80b4) and ENDF/B-VII.1 with blue (e71).

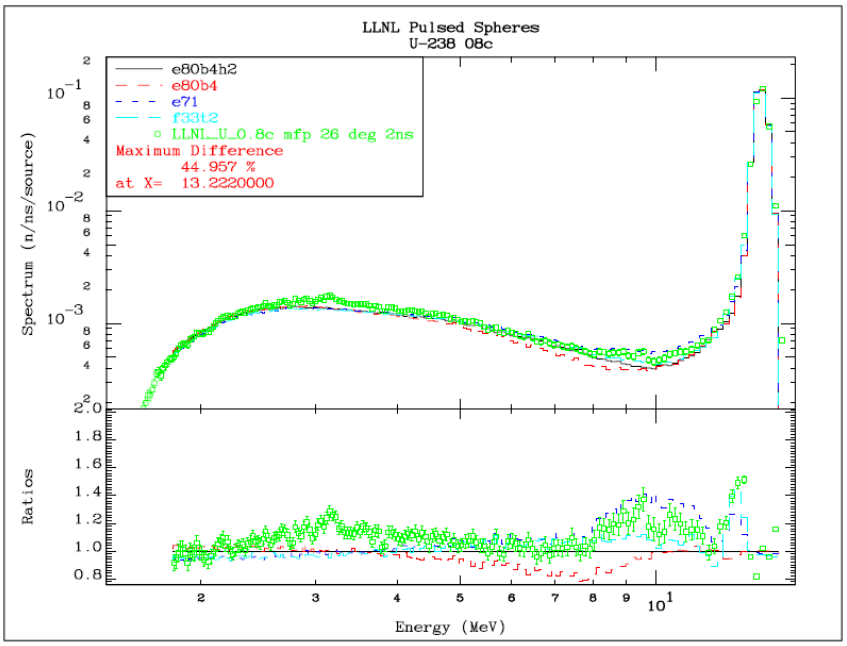

Figure 21: Comparison of neutron spectrum measurements to reference benchmark model calculations for experimental configuration 08c. Measurements are marked with green, reference calculations performed with ENDF/B-VIII.0 β4+ data library are marked with black color (e80b4h2), calculations performed with a previous version of ENDF/B-VIII.0 β4 are marked with red (e80b4) and ENDF/B-VII.1 with blue (e71).

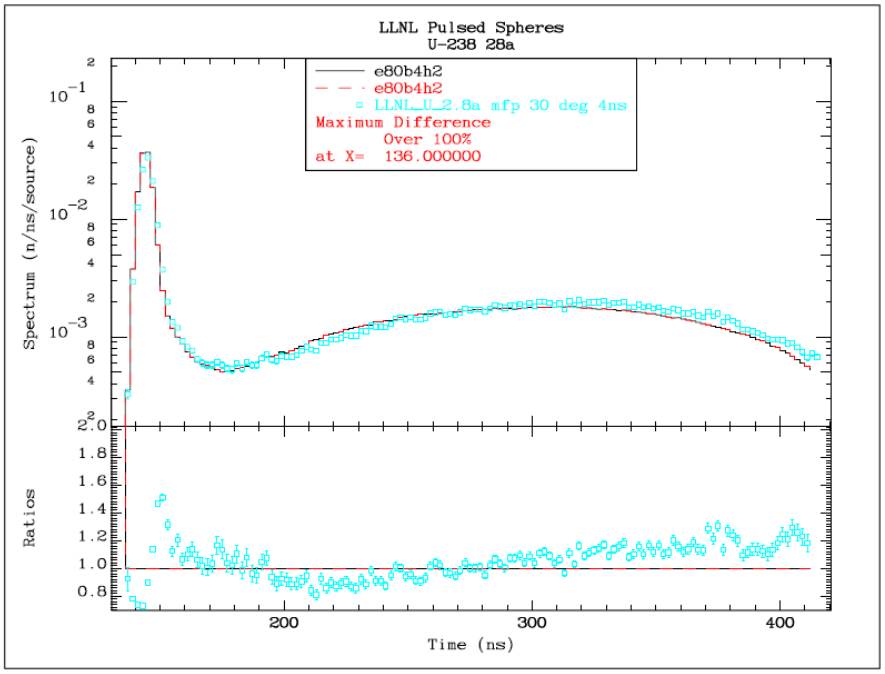

Figure 22: Comparison of time of flight measurements to reference benchmark model calculations for experimental configuration 28a. Measurements are marked with light blue and reference calculations with black and red color.

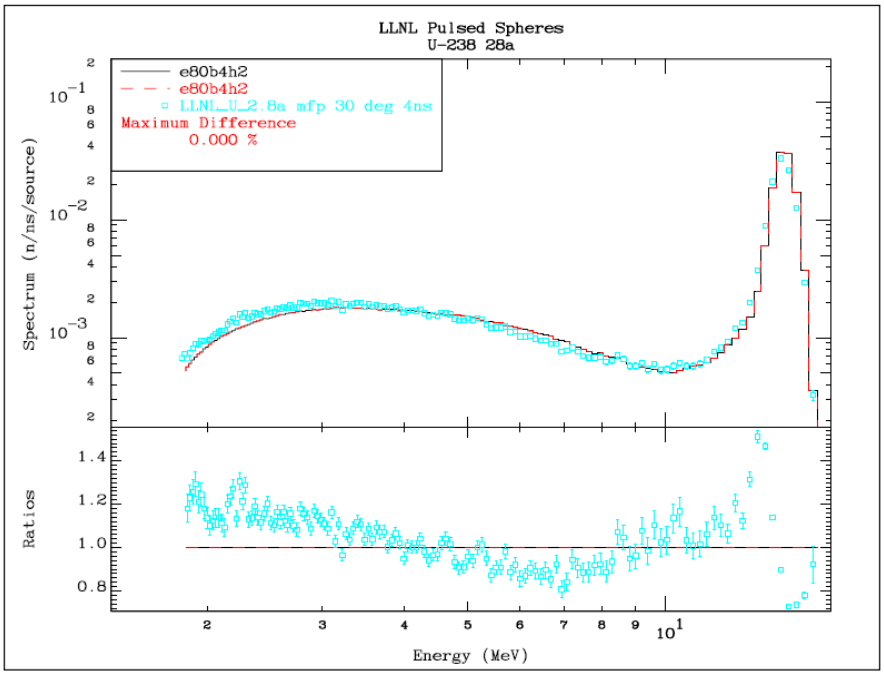

Figure 23: Comparison of neutron spectrum measurements to reference benchmark model calculations for experimental configuration 28a. Measurements are marked with light blue and reference calculations with black and red color.

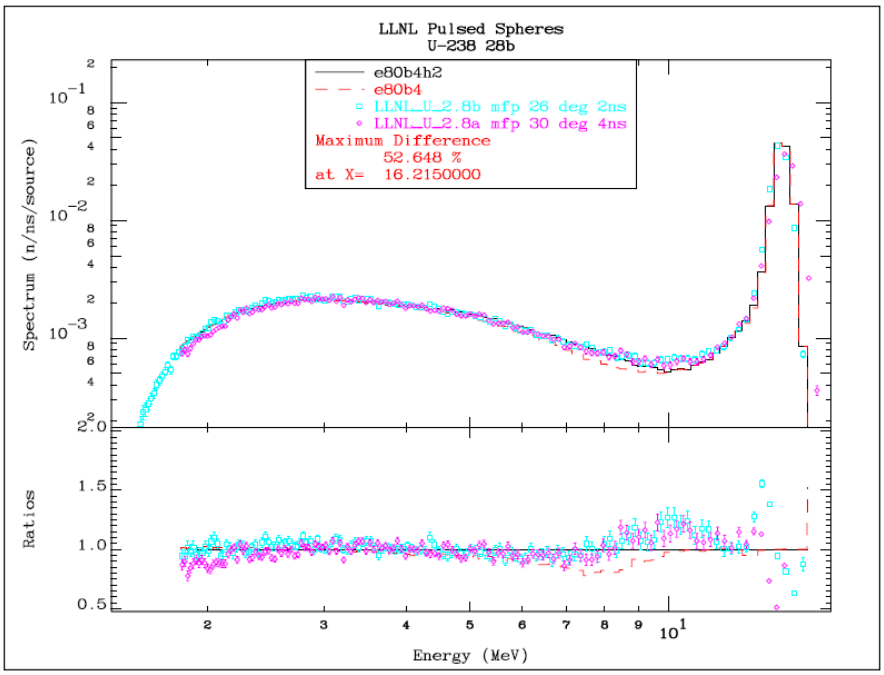

Figure 24: Comparison of neutron spectrum measurements with neutron detectors at different angles to reference benchmark model calculations for experimental configuration 28b. Measurements are marked with light blue (26°) and magenta (30°) and the reference calculations for the 26° detector with ENDF/B-VIII.0 β4+ data library marked with black and calculations with ENDF/B-VIII.0 β4 marked with red color.

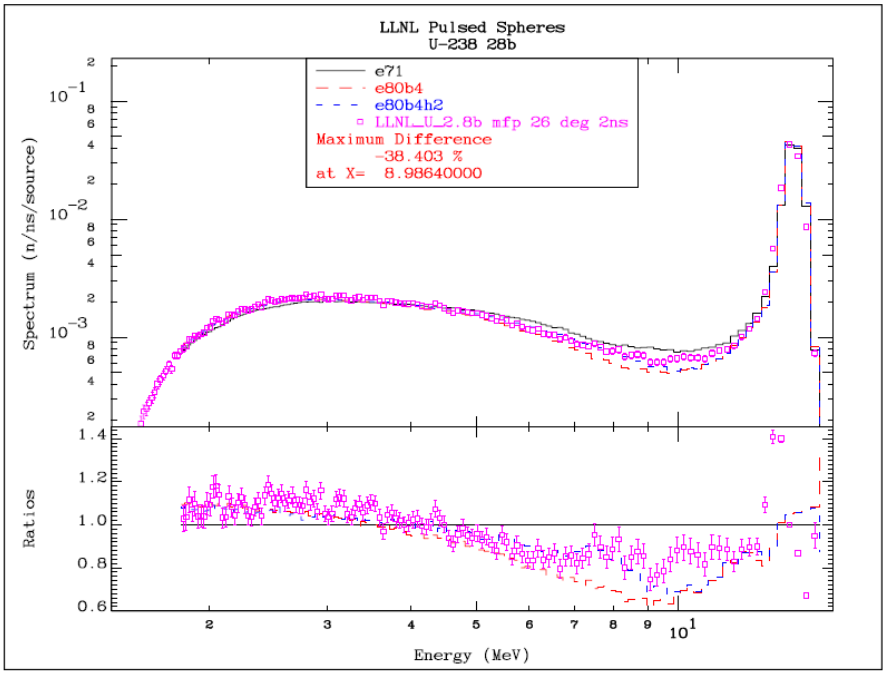

Figure 25: Comparison of neutron spectrum measurements to reference benchmark model calculations for experimental configuration 28b. Measurements are marked with magenta, reference calculations performed with ENDF/B-VII.1 data library are marked with black color, calculations with ENDF/B-VIII.0 $\beta 4+$ data library are marked with blue color (e80b4h2) and calculations performed with a previous version of ENDF/B-VIII.0 $\beta 4$ are marked with red (e80b4).

5.2 Sensitivity to flight path length

No information about the reference point for flight path length measurements was found. It could be measured to the beginning, middle or end of the active part of the neutron detector. Therefore sensitivity of the results to the flight path length was evaluated. Flight paths for all evaluated ^{238}U spherical configurations were changed for $\pm$ 10 cm and results were compared to the unperturbed calculations. Compared results are presented in Figures 26 - 30. It was concluded that the uncertainty in the flight path has negligible effect on the detected neutron spectra.

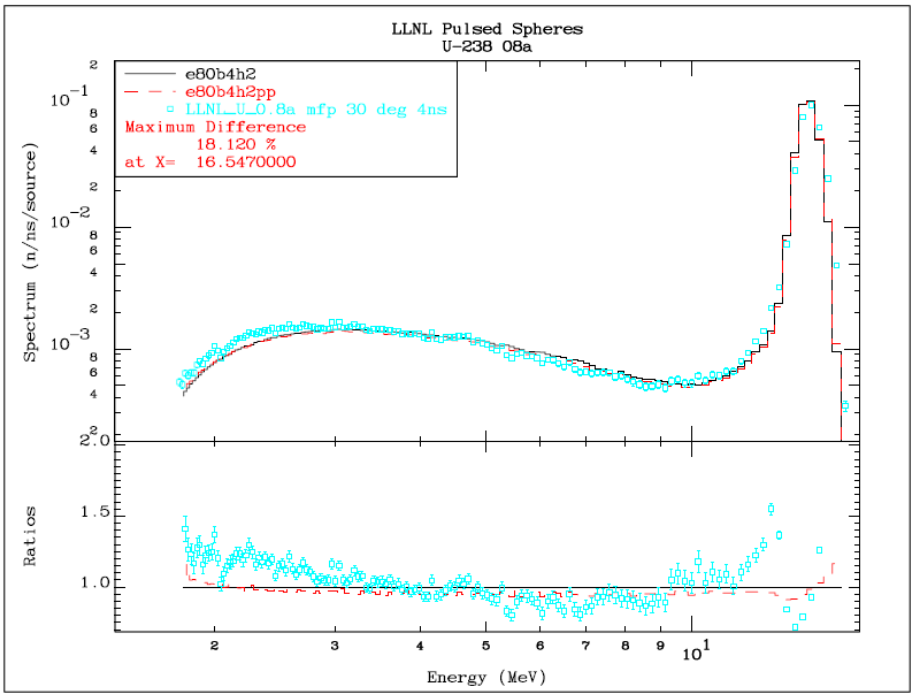

Figure 26: Evaluated sensitivity to the flight path length for experimental configuration 08a. Measurements are marked with light blue, reference results are marked with black color and results for changed flight path for +10 cm with red.

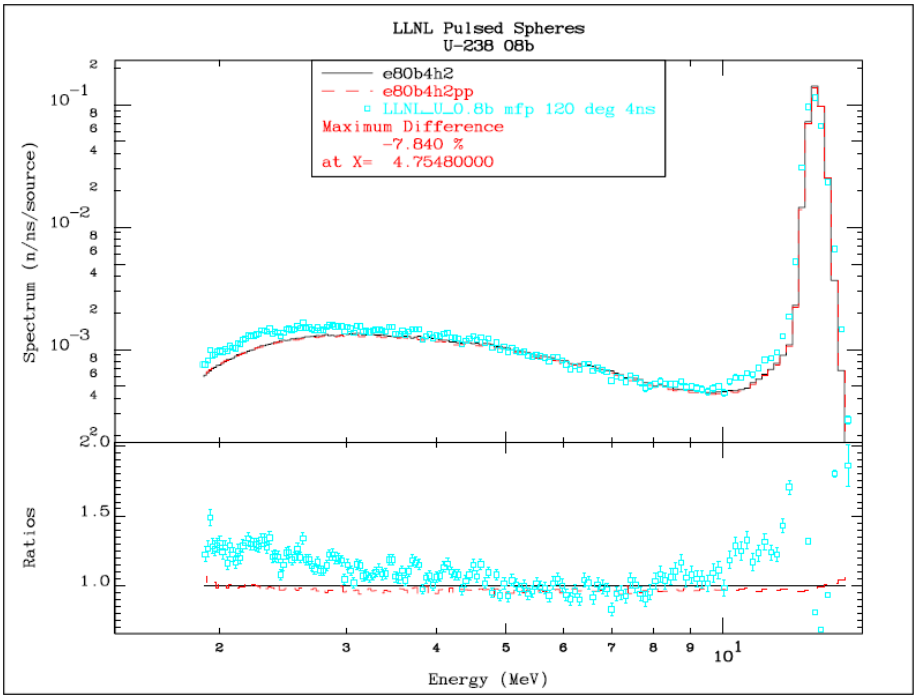

Figure 27: Evaluated sensitivity to the flight path length for experimental configuration 08b. Measurements are marked with light blue, reference results are marked with black color and results for changed flight path for +10 cm with red.

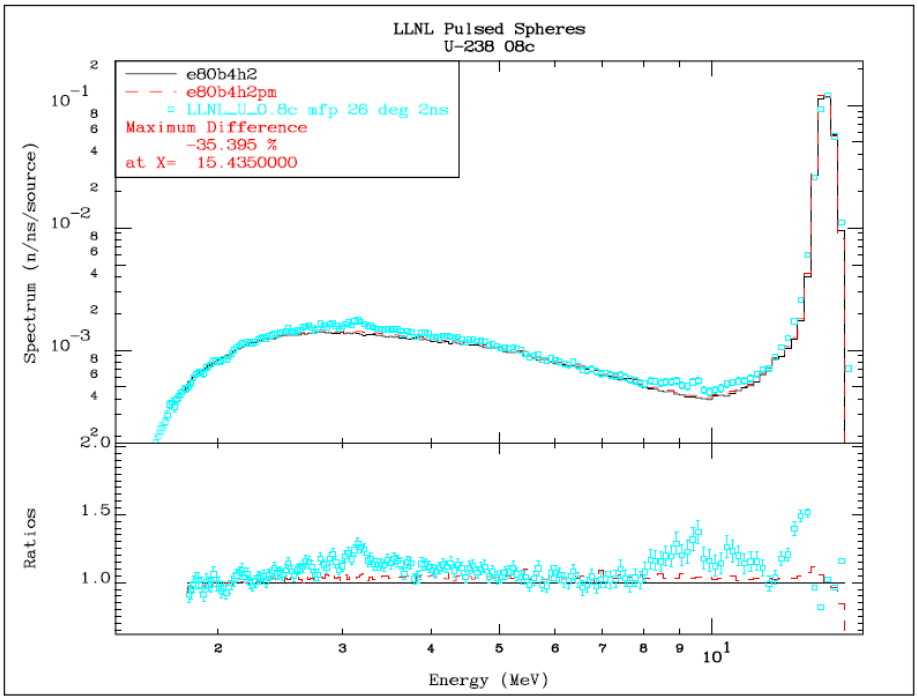

Figure 28: Evaluated sensitivity to the flight path length for experimental configuration 08c. Measurements are marked with light blue, reference results are marked with black color and results for changed flight path for -10 cm with red.

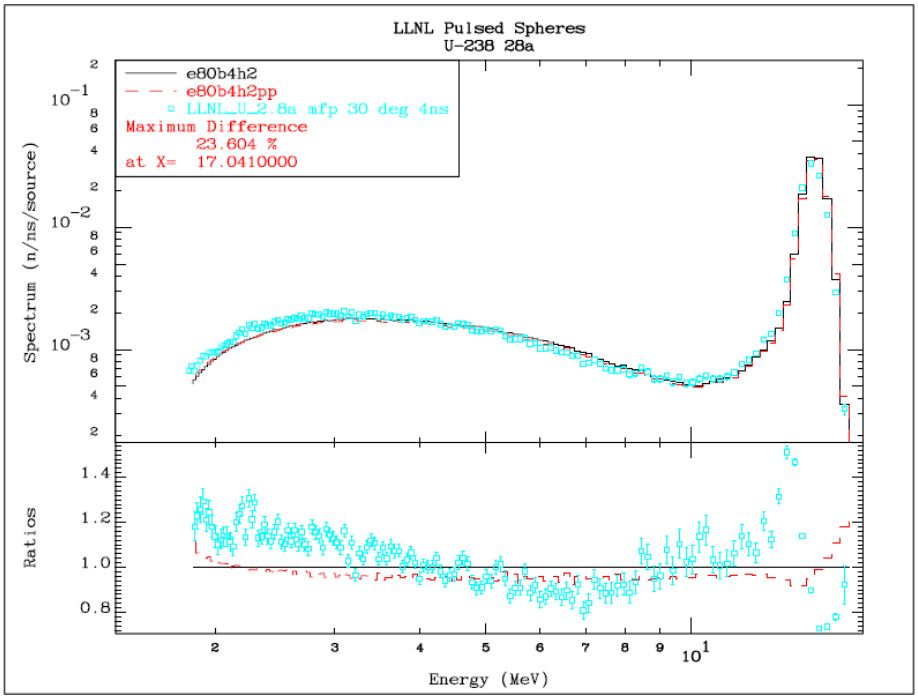

Figure 29: Evaluated sensitivity to the flight path length for experimental configuration 28a. Measurements are marked with light blue, reference results are marked with black color and results for changed flight path for +10 cm with red.

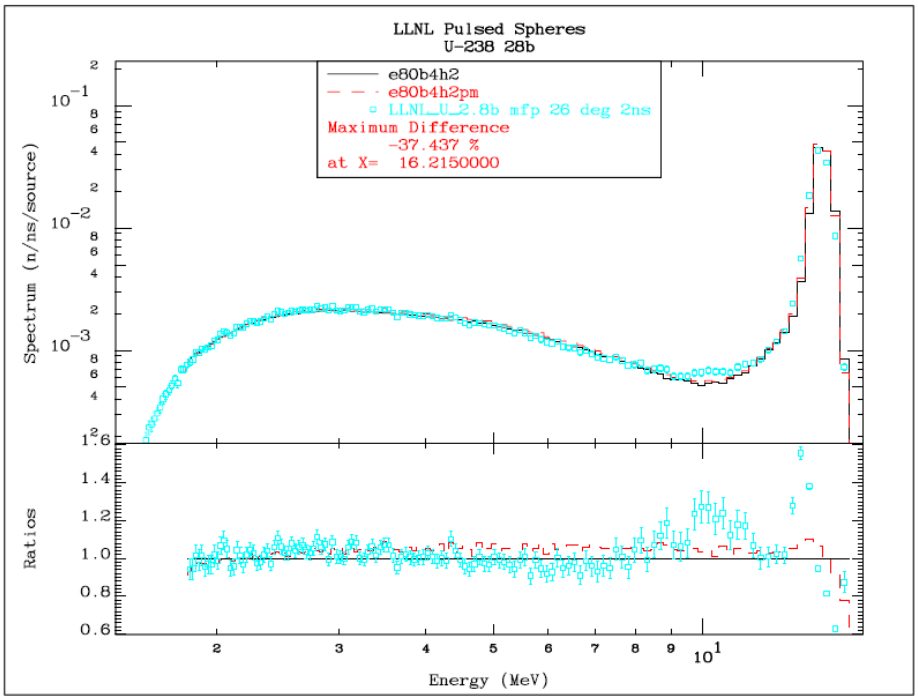

Figure 30: Evaluated sensitivity to the flight path length for experimental configuration 28b. Measurements are marked with light blue, reference results are marked with black color and results for changed flight path for -10 cm with red.

5.3 Sensitivity to detector angle

The sensitivity of the results on the detector angle was also studied. Considering different schematic drawings of experimental configurations it was inconclusive whether the reported angles (30° and 120° were measured from the incident deuteron beamline or from the 26° detector beamline. The effect was evaluated for the 30° detector. Its angle was changed for approximately 5° from approximately 39° to 34°. The results can be observed in Figure 31, where calculations at different detector angles (black color represents reference calculation and red color represents calculations with changed detector angle for 5°) are compared to the experimental results (light blue). It can be concluded that the uncertainty in the detector angle has a negligible effect especially in the lower energy region where the deviations between the experiment and calculations are the highest.

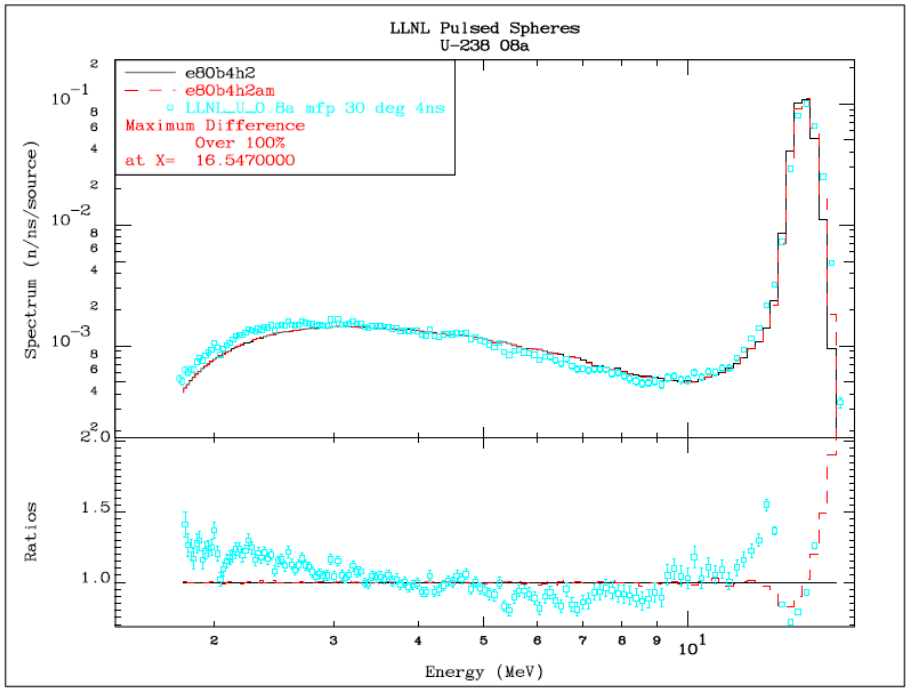

Figure 31: Evaluated sensitivity to the detector angle (-5°) for experimental configuration 08a. Measurements are marked with light blue, reference results are marked with black color and results for changed detector angle with red.

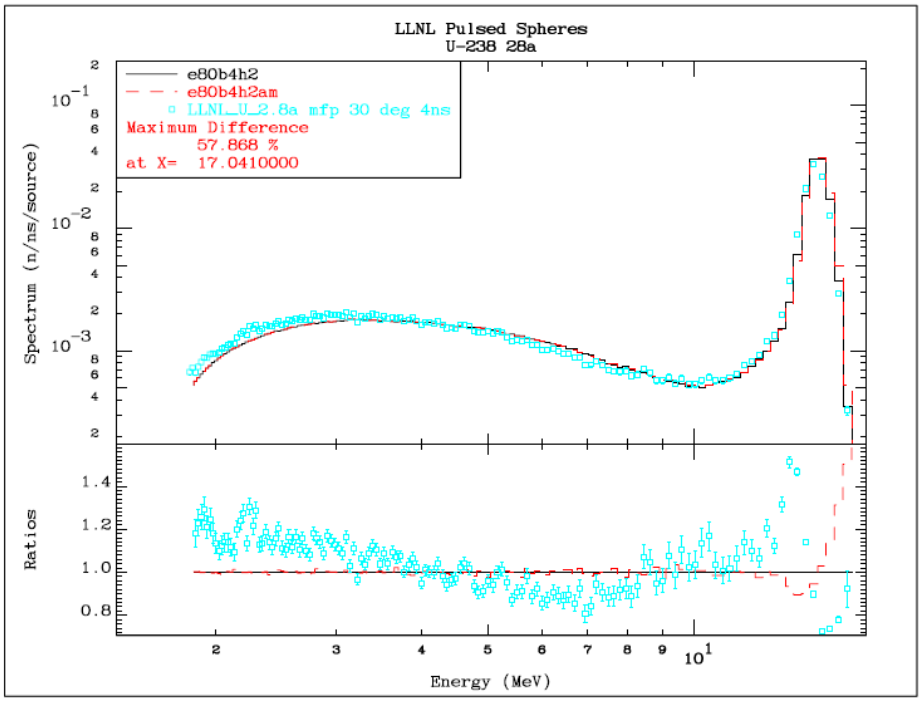

Figure 32: Evaluated sensitivity to the detector angle (-5°) for experimental configuration 28a. Measurements are marked with light blue, reference results are marked with black color and results for changed detector angle with red.

5.4 Sensitivity to the concrete layer surrounding beamline

Due to the geometry simplifications in the reference computational model the concrete walls and collimators were not modelled explicitly. To account for that beamlines were surrounded with a thin layer of concrete with neutron importance set to 0, which means they were actually modelled as black absorbers. We changed their neutron importance back to 1 to evaluate the effect of modelling them as concrete or as black absorbers. High differences (∼20 %) between both calculations can be observed in Figure 33. Due to the not explicitly modelled geometry it is not possible to determine which evaluation is more accurate. Modelling concrete surrounding the beamline as black absorber should compensate for the effect of not modelling the collimator. Therefore we decided to also perform the calculations with explicitly modelled experimental geometry and collimators within the wall, which is evaluated in the Section 5.6.

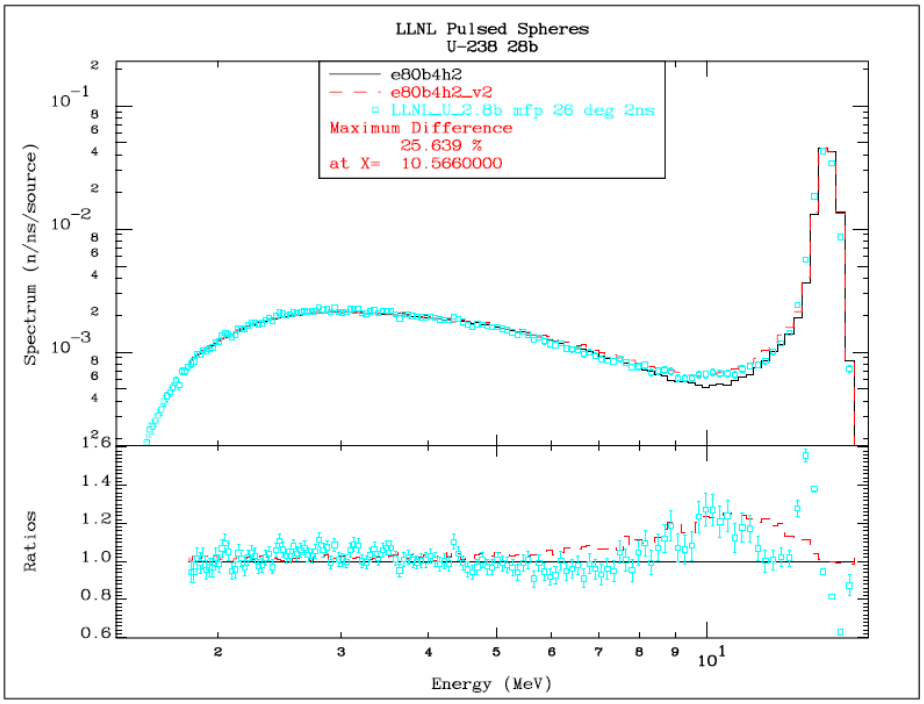

Figure 33: Evaluated sensitivity to the concrete layer surrounding the beamline for experimental configuration 28b. Measurements are marked with light blue, reference results are marked with black color and results for changed importance of concrete surrounding the beamline are in red.

5.5 Sensitivity to the normalization *sphere in/sphere out*

In reference [7], evaluating the Monte Carlo TART calculations is described: *Unfortunately, black experiments are not available in the disp93in file. However, there exist published figures showing the results of blank runs, and we used them for comparison. For example, Fig. 4 from the 1990 paper by Goldberg, et al.*[1]*, shows the blank neutron spectrum for flight path of 852.5 cm measured with NE213 scintillator. This figure was scanned and digitalized.* The scanned version along with the TART calculation normalized and corrected for detector efficiency, from the reference [7] is reproduced as Figure 34. Reference [7] states: *The small peak appearing in the experimental data at 350 ns corresponds to 2.81 MeV neutrons from the reaction* $^2H(d,n)^3He$ *resulting from the deuterium build-up in the tritium target.*

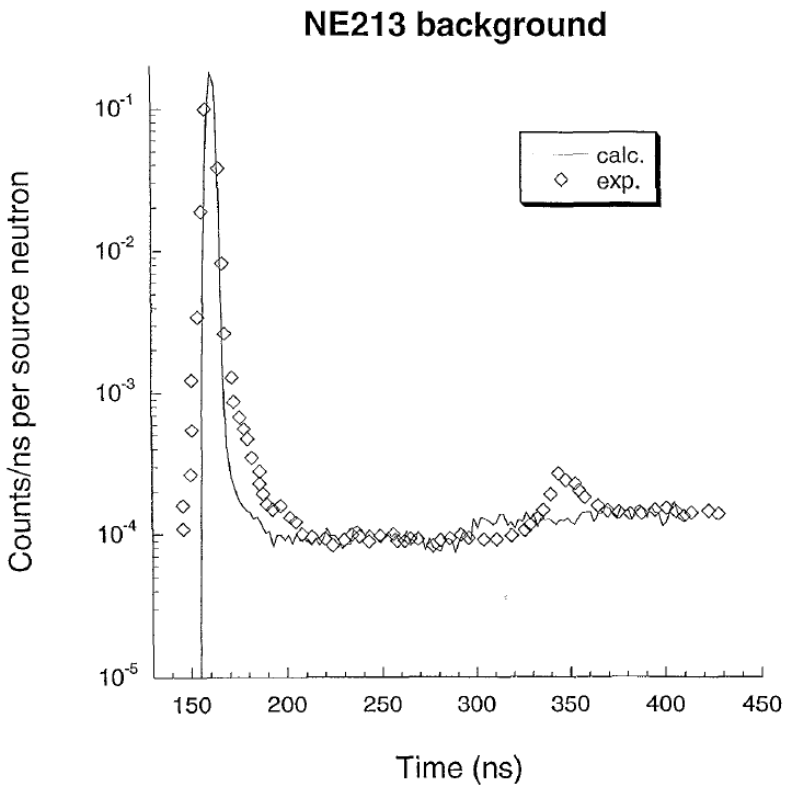

Figure 34: Comparison between calculated (TART) and experimental neutron background spectra with the NE213 scintillator at a bias of ∼0.8 MeV [7].

The statement that the measured neutron spectra with target in (sphere) were normalized to the target out (sphere removed) is supported in many references through different statements. In reference [6] is reported: *The measured data for each spherical assembly ("target in") was normalized to the total flux measured with the material of interest removed from the spherical assembly ("target out").*

In reference [3] is stated: *The experiment consist of recording the ratio of counts with the sphere material in to counts with the sphere material out. With this differencing technique, the effects of the low-mass target assembly, the detector collimator and the air in the flight path between the target and the detector essentially cancel out, and hence have no significant effect on the experimental data. In particular, with the sphere out, the counting rate from neutrons which are scattered from the target assembly and collimator is three orders of magnitude less than the counting rate from the uncollided*

[1] E. Goldberg, et al., Nucl. Sci. Eng., 105, 319 (1990)

neutron beam. Therefore, only the portions of the sphere-in neutron spectrum that have three-order-of-magnitude peak-to-valley changes in the counting rate will be affected. The largest effects are for the strongly-forward-peaked heavy elements - Pt, ^{235}U, ^{238}U *and* ^{239}Pu.

Reference [5] describes: *Because we used target-in/target-out technique, only the relative neutron production had to be determined. This value was obtained from the ratio of total neutron counts in the detector to total number of alpha particles detected during target-out accelerator run. Thus, the relative neutron source strength during the target-in run is the product of the relative neutron production and the integral alpha count.*

In reference [2] is stated: *Since the high-energy pulsed sphere measurements are essentially transmission experiments (i.e.* $\frac{I}{I_0}$*, the ratio of intensities with and without spherical targets), the only requirement is a relative monitor of the neutron production. In other words, the sphere-in and sphere-out measurements must be for the same neutron production (same* ^4He *counts), the absolute neutron production being unimportant. In practice the sphere-out measurements, being run for fewer* ^4He *counts, were normalized to the* ^4He *counts for the sphere in measurements.* $\frac{I}{I_0}$ *has units of neutron counts per nsec divided by total 14-MeV counts with the sphere removed. Using the relative detector efficiency as a function of neutron energy and the angular distribution of the source neutrons,* $\frac{I}{I_0}$ *can be converted to neutrons per nsec per source neutron. Hence neutrons per nsec per source neutron can be measured without knowing either the absolute neutron production or the absolute detector efficiency.*

As indicated in the last citation the I_0 are total 14-MeV counts with the sphere removed. Because this number is an integral and was applied through the entire energy range, the shape of the energy spectrum remains unchanged and the effect was therefore considered irrelevant and was not applied in the calculations.

By comparing calculated and measured neutron spectra without the sphere in Figure 34, it can be observed that the Marchetti's neutron source is not completely describing the measurements. It can be noted that the peak width is not in complete agreement and that at the bottom of the peak some deviations occur, which imply that the neutron source is not precisely known. Moreover, there is additional peak visible at the ∼2.8 MeV that can significantly effect the results below ∼4 MeV. **Therefore the comparison of experiments and calculations below 4 MeV is considered less reliable.** It should be noted that this additional peak is not taken into account in the current MCNP model of the neutron source.

5.6 Detailed computational model

The impact of not explicitly modelled experimental geometry was determined by performing calculations with a detailed computational model. A MCNP input of the detailed model is listed in Appendix A. In the detailed computational model the experimental configuration was explicitly modelled. The schematic view of the modelled geometry in the detailed MCNP model is presented in Figure 35. Detectors were not modelled as rings but as volume detectors. In addition also concrete pit was added with modelled holes and collimators inside the wall. Concrete pit was modelled with 10.24 m distance between the inner walls and with 2.02 m wall thickness, same as the Mercury model (see Figure 12). There was no reported thickness of the aluminium floor in the references, only that it was low-mass aluminium. However, it was assumed that its effect on the detector signal is minimum and was modelled 38 cm thick. The ceiling was modelled opened. Cone shaped collimators inside the beamline in the wall were modelled according to the technical drawing presented in Figure 2 and can be observed in Figure 36.

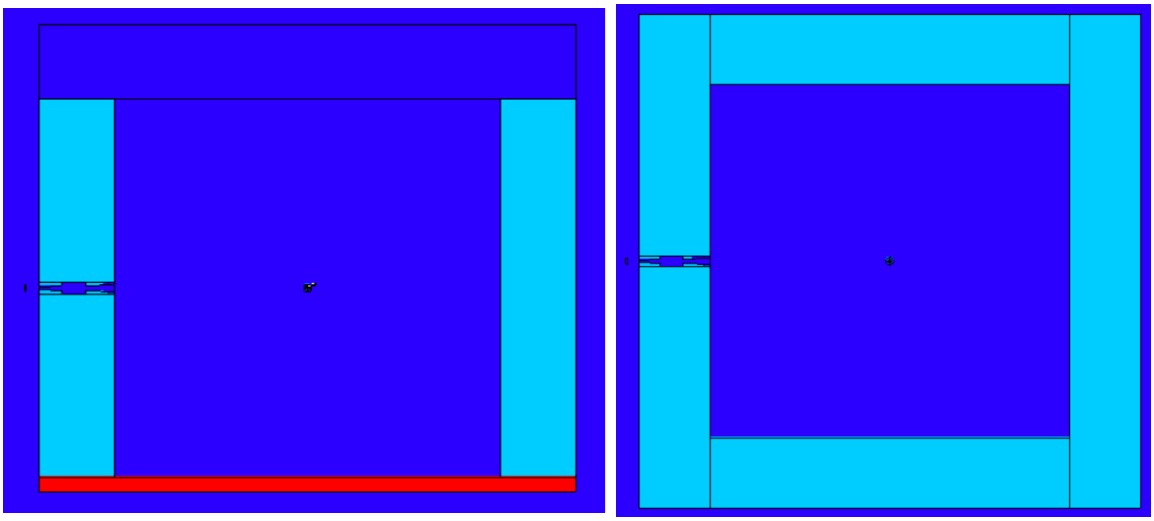

Figure 35: View of the detailed MCNP computational model geometry in the xz-plane (left) and xy-plane (right) view. Dark blue color represents air, light blue color concrete walls and red color aluminium floor.

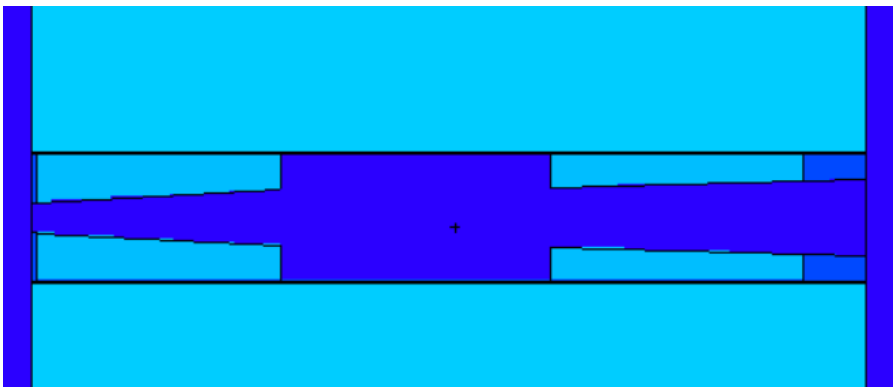

Figure 36: View of the beamline and collimators inside the wall for 26° beamline in the detailed MCNP model.

Contrary to the reference MCNP model in the detailed model the coordinate system was positioned so that the z-axis was positioned perpendicular to the floor as can be observed in Figure 37. The incident deuteron beam was modelled forming 26° angle with the floor and was modelled with the same geometry as in the reference model. The 26° beamline was modelled in line with the center of the sphere and straight through the wall.

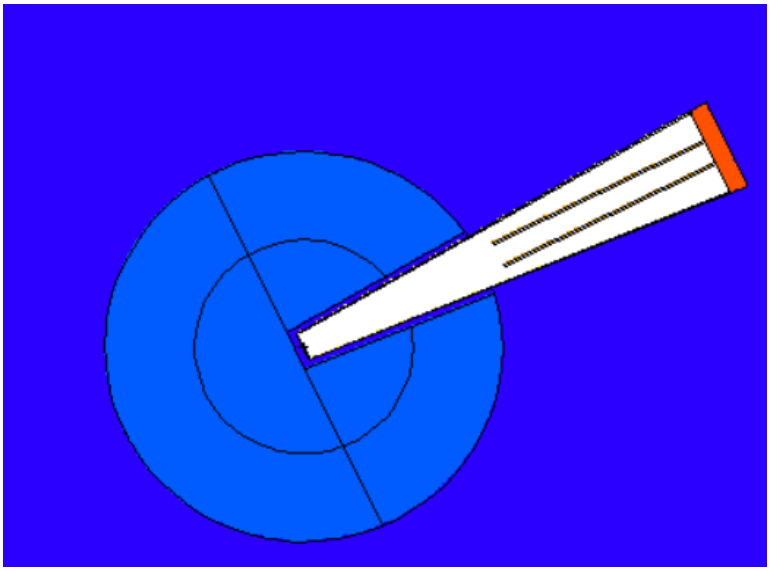

Figure 37: View of the large (2.8 mfp) ^{238}U sphere with incident deuteron beamline in the detailed MCNP model.

Due to the smaller detector angle the calculations with detailed model took large amount of computer-time and were therefore performed only for one experimental configuration to demonstrate the impact of simplifications in geometry on the detected neutron spectra. In Figure 38 the results of the detailed model are compared with a reference calculation and experiment. All spectra were normalized taking into account only energies above 4 MeV, due to the missing source peak at ∼2.8 MeV in the MCNP model as explained in Section 5.5. It can be observed that around the local minimum (at ∼10 MeV) calculations with a detailed model give similar results as the reference calculations and do not agree well with measurements. This leads to the conclusion that the reference MCNP model can be considered acceptable even thought some geometry simplifications were made. This also confirms that the good agreement in case of the effect of the concrete layer (marked with red color in Figure 38 and evaluated in Section 5.4) is only random. In addition some deviations between the calculated spectra with a detailed model and the experimental results in the lower energy region (around 3 MeV) can be observed. This can be due to the not correctly modelled neutron source as discussed in Section 5.5 and should not be taken into account.

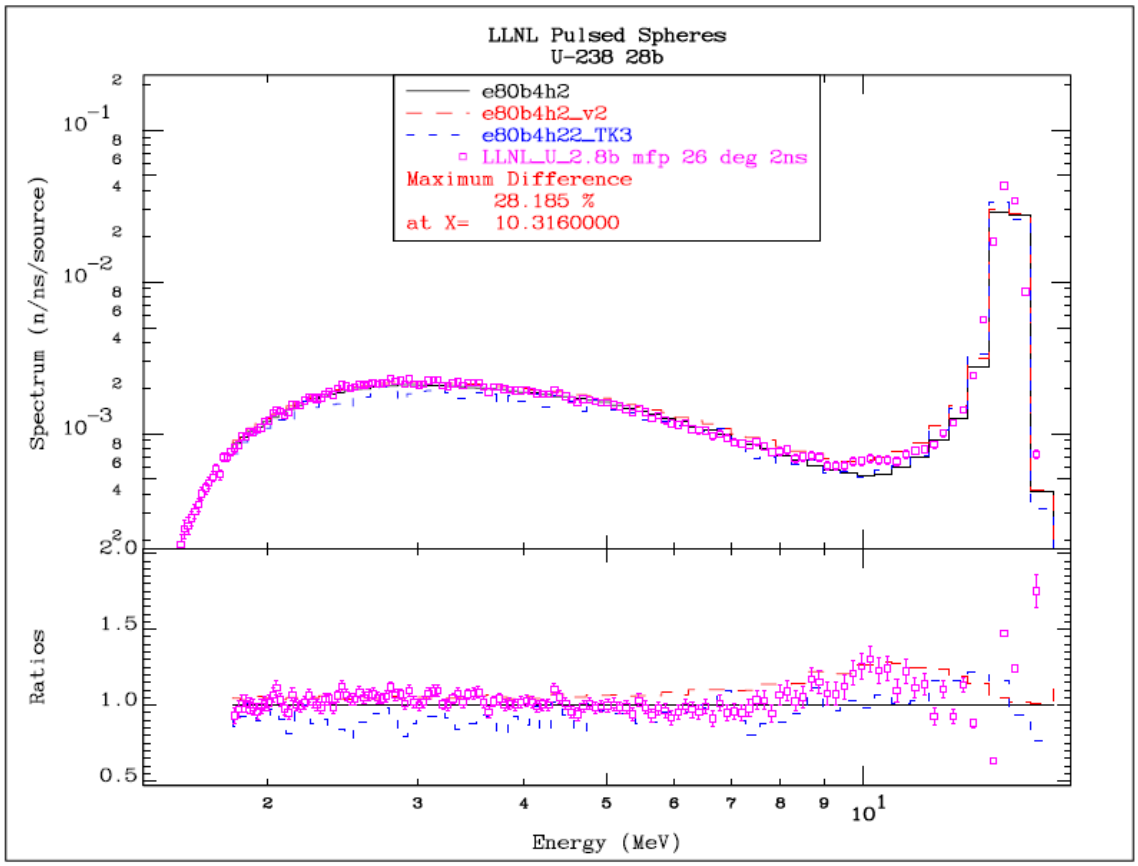

Figure 38: Evaluated sensitivity to the not explicitly modelled experimental geometry for experimental configuration 28b. Measurements are marked with magenta, reference results are marked with black color (e80b4h2), results for changed importance of concrete surrounding the beamline are in red (e80b4h2_v2), results with detailed model are marked with dark blue (e80b4h22_TK3).

6 Conclusion

This report describes the evaluation of the analysis of the ^{238}U Livermore Pulsed Sphere experiments relevant for the validation of the CIELO evaluations. The aim was to validate the new ENDF/B-VIII.0 nuclear data library by comparing calculations to the benchmark experiments. The references describing the experimental configuration or computational models for the pulsed sphere experiments were reviewed. Experiments were performed with two ^{238}U spheres of different diameters: 0.8 mfp and 2.8 mfp. Experiments found in different references and experiments included in the evaluation are listed and their characteristics are reported. Experiments were performed using neutron detectors (Pilot-B or NE213 scintillators) behind collimators and concrete wall. These detectors were positioned in different directions in regard to the incident deuteron beamline: 26°, 30° and 120°. The discussion about the reported angles is included in the report. The reference model used for calculations was from Stephanie C. Frankle. When comparing calculated detected neutron spectra to the experimental results the differences between different configurations were observed. The deviations between different experimental configurations and different detectors were inconsistent and therefore made conclusions about the accuracy of the new nuclear data libraries difficult. To determine the reason for the deviations, the geometry simplifications (e.g., ring detector) included in the reference model were investigated and sensitivity analysis was performed. It was concluded that the path length and detector angle have negligible effect on the detected neutron spectrum. On contrary, the concrete surrounding the beamline has high impact on the neutron spectrum. For evaluating the bias due to the not explicitly modelled geometry the detailed computational model with Monte Carlo neutron transport code MCNP was made. Detailed model included also an explicitly modelled concrete pit with beamline holes and collimators inside. It was concluded that the results show some inconsistency, which is comparable to the order of magnitude of the statistical uncertainty of the calculations and therefore can not be used to evaluate the differences between the different versions of the new versions of the nuclear data library evaluations. It was also concluded that due to the not correctly modelled neutron source in the MCNP model (D-D peak at ∼2.8 MeV is not included in the neutron source) the comparison below ∼4 MeV is less reliable.

7 References

[1] Dermott E. Cullen, A Pulsed Sphere Tutorial, LLNL-TR-726839, Lawrence Livermore National Laboratory, 30.1.2017.

[2] C. Wong, et al., Livermore pulsed sphere program: program summary through July 1971, UCRL-51144, Lawrence Livermore Laboratory, February 1972.

[3] E. F. Plechaty and R. J. Howerton, Calculational models for LLL Pulsed Spheres (CSEWG Shielding Benchmark Collection No. STD 19), UCID-16372, Lawrence Livermore Laboratory, October 1973.

[4] W. W. Webster, P. S. Brown, Low energy time-of-flight spectra from spheres pulsed by 14-MeV neutrons, UCID-17223, Lawrence Livermore Laboratory, August 1976.

[5] W. Webster, C. Wong, Measurements of the neutron emission spectra from spheres of N, O, W, ^{235}U, ^{238}U and ^{239}Pu pulsed by 14-MeV neutrons, UCID-17332, Lawrence Livermore Laboratory, December 1976.

[6] R. D. Mosteller, S.C. Frankle, P. G. Young, Data testing of ENDF/B-VI with MCNP: critical experiments, thermal-reactor lattices, and time-of-flight measurements, LA-UR-96-2143, Los Alamos National Laboratory, 1996.

[7] A. A. Marchetti and G. W. Hedstrom, New Monte Carlo Simulations of the LLNL Pulsed-Sphere Experiments, UCRL-ID-131461, Lawrence Livermore National Laboratory, July 1998.

[8] L.F. Hansen, et al., Updated summary of measurements and calculations of neutron and gamma-ray emission spectra from spheres pulsed with 14-MeV neutrons, UCID-19604, Lawrence Livermore National laboratory, 1989.

[9] J. A. Bucholz and S. C. Frankle, Improving the LLNL Pulsed Sphere Experiments Database and MCNP Models, LA-UR-03-0609, Los Alamos National Laboratory, June 2003.

[10] R. Procassini and M. S. McKinley, Modern Calculations of Pulsed-Sphere Time-of-Flight Experiments Using Mercury Monte Carlo Transport Code, Joint International Conference on Supercomputing in Nuclear Applications and Monte Carlo 2010 (SNA + MC2010), Hitotsubashi Memorial Hall, Tokyo, Japan, October 17-21, 2010.

[11] Goorley, T., et al., 2012. Initial MCNP 6 Release Overview. LA-UR-11-07082, Los Alamos National Laboratory, also Nuclear Technology, 180, pp. 298-315 (Dec 2012).

[12] S. C. Frankle, LLNL Pulsed Sphere Measurements and Detector Response Functions (U), LA-UR-05-5878, Los Alamos National Laboratory, January 2004.

Appendices

A Detailed MCNP model input

Listed is the input of the detailed model for the Monte Carlo neutron transport code MCNP [11]. This model includes explicitly modelled concrete pit with a 26° beamline hole with collimator in the wall. The detector response is calculated through 3 different tally types: volume, surface and point detector. To achieve the reliable statistics for volume and surface detectors the input was run with approximately $8{\cdot}10^9$ source neutrons.

```
28u2.8b:  U-238, 2.8 mfp, fwhm=2.0 ns, NE213-B bias=1.6, FP=746.34 cm,  26-deg
c
c    U-238 Sphere, 2.8 mfp, Detailed model by Tanja Kaiba, July 2017
c
c    ******************************************************************************
c    ******************************************************************************
c    **
c    **  Geom/Matl model:  238U2.8
c    **
c    **  Orig Ref/Figure:  See page 81 of "Measurements of the Neutron Emmission
c    **                    Spectra From Spheres of N, O, W, U-235, U-238, and Pu-239,
c    **                    Pulsed by 14-MeV Neutrons," UCID-17332 (Dec 1976)
c    **
c    **  Some Orig Specs:  Mass is not given
c    **                    Den(U)=19.04 g/cc (99.0 at% U-238)
c    **
c    **  Size:  2.8 mfp (appx);  Rmax=10.932 cm
c    **
c    **  E-Image:  (not available)
c    **
c    ******************************************************************************
c    ******************************************************************************
c    **
c    **  Depending on the pulse width (fwhm), detectors of interest would include:
c    **
c    **  If pulse=4.0 ns, 28u2.8a=  Pilot-B  (Bias=1.6)  Path=765.2  cm,  30-deg line
c    **  If pulse=2.0 ns, 28u2.8b=  NE213-B  (Bias=1.6)  Path=746.34 cm,  26-deg line
c    **
c    ******************************************************************************
c    ******************************************************************************
c    **
c    **  This is the FINAL detailed geometrical model of the experimental geometry.
c    **  It was produced to evaluate the bias due to the geometrical simplifications
c    **  in the reference input.
c    **  Concrete pit walls, 26deg beamline hole through the wall and collimator
c    **  inside hole were modelled. Incident deuteron beamline is forming 26deg angle
c    **  with the aluminum floor. In input _TK3.i changes to the neutron source
c    **  surface angle were made to compensate for the different coordinate system
c    **  as in the reference model.
c    **  Detector response is calculated using F4 (volume) tally. The detector
c    **  energy response functions remained the same as in the reference model.
c    **  Surface tally (F2 type) was added for comparing the results to the
c    **  volume tally.
c    **
c    **  Added point detector tally.
c    **
c    **  Different random number generator as in _TK3.i is used for multiple
c    **  individual runs.
c    **  Modification made by Tanja Kaiba, 24.7.2017
c    **
c    ******************************************************************************
c    ******************************************************************************
c
c    BEGIN CELLS:
c    ------
c    m514 = 19.04 g/cc    =  U-238 metal, nominally at 19.04 g/cc
```

```
c    m501 = 0.001288 g/cc =  Air, nominally at 0.001288 g/cc
c    ------
1    514 -19.04     -1 -3    trcl=1
2    514 -19.04     -1  3 -4 trcl=1
3    514 -19.04      1  2 -3 trcl=1
4    514 -19.04      1  2  3 -4 trcl=1
5    501 -0.001288   1 -2 -4    #(-101 -111 103) trcl=1 $ exclude target assembly
6    501 -0.001288   4 -207 208 -209 210 -211 212 #105 #106 #107 #108 $ exclude target assembly
7    0               99             $ outside world
8    501 -0.001288 -99 #(-201 202 -203 204 -205 206) #400 $ air outside concrete pit
c
c
c    New cells for target assembly (see Fig 6 in UCRL-51144, Rev I):
c    ---------------------------------------------------------------
c    m581 =  1.879497 g/cc = Target Material  (50 at% Tritium, 50 at% Titanium), nominally at 1.879497 g/cc
c    m582 = 30.073815 g/cc = Target Component (all Tungsten), artificially at 30.073815 g/cc in model
c    m583 = 20.096000 g/cc = Target Component (mostly Iron and Copper), artificially at 20.096000 g/cc in model
c    m584 = 23.180464 g/cc = Target Component (AL, H, and C) artificially at 23.180464 g/cc in model
c    m585 =  2.701353 g/cc = Target Component (all Aluminum), nominally at 2.701353 g/cc in model
c    m586 =  2.705809 g/cc = Target Component (all Aluminum), nominally at 2.705809 g/cc in model
c    m587 = 20.008000 g/cc = Target Component (Aluminum and Copper) artificially at 20.008000 g/cc in model
c    ------
c    Note:  The recommended densities given here have been artificially adjusted so that, when used in
c    combination with the stated geometry (see Fig 6 in the following reference), MCNP will faithfully
c    reproduce the actual masses in each target assembly zone, as also given on Fig 6 of that reference.
c    ------
c    Taken from Fig. 6 (on page 10) of "Livermore Pulsed Sphere Program:
c    Program Summary Through July 1971", UCRL-51144, Rev I (Feb 10, 1972);
c    also shown as Fig. 2 of Ham Hunter's SINBAD Experiment SBE 17.001 file.
c    ------
101  583 -20.096000   -101  -104   103  trcl=1 $ tip of target assembly; zone 3 (Alloy, mass=1.100 grams) in Fig 6
102  582 -30.073815   -101  -105   104  trcl=1 $ zone 2 (Tungsten, mass=3.25 grams) in Fig 6
c    cel  mat   den   -112  -107   106  trcl=1 $ pure tritium region "if" it were modeled explicitly (but it's not)
103  581  -1.879497   -101  -108   105  trcl=1 $ homog targ, zone 1 (50 at% T, 50 at% Ti, mass=0.004 grams) in Fig 6
104  584 -23.180464   -101   102  -115   108   trcl=1 $ zone 4 (AL,H,C alloy ring, mass=1.5 grams) in Fig 6
105  585  -2.701353   -101   102  -110   115   trcl=1 $ zone 5 (outer AL body of assy, mass=35.6 grams) in Fig 6
106  587 -20.008000   -101  -111   110         trcl=1 $ zone 7 (AL+Cu assy backplate, mass=417.0 grams) in Fig 6
107  586  -2.705809   -114   113  -110   109   trcl=1 $ zone 6 (part-length AL cyl in assy, 18.3 grams) in Fig 6
108  0               (-102  -110   108) #107   trcl=1 $ sealed vacuum inside the target assembly
c    excl zone  #(-101 -111 103)   $ exclusion zone for target assembly, to be used in base model
c    ---------------------------------------------------------------
c
c   26 deg beam line
c   -----
301  589 -7.87 -302 301 -208 202     $ Fe guide tube inside wall
302  589 -7.87 -301 -208 303 304     $ Fe colimator #1
303  501 -0.001288 (-208 305 -303):(-301 -305 306):(-307 -306 308) &
                  :(-308 202 -309) $ air inside colimator
304  590 -1.35 -301 303 -304 305     $ borated paraffin collimator #2
305  590 -1.35 -301 307 -306 308     $ borated paraffin collimator #3
306  589 -7.87 -308 202 -301 309     $ Fe at the end of collimator
c   -----
c    Room - concrete pit
c    material: m521 with isotopic composition and density as in previous input
c    floor material: aluminum
c    ------
201  521 -2.35 -201 207 -203 204 -211 212  $ concrete wall #1
202  521 -2.35 202 -208 -203 204 -211 212 #301 #302 #303 #304 #305 #306 $ concrete wall #2
203  521 -2.35 -203 209 -207 208 -211 212  $ concrete wall #3
204  521 -2.35 204 -210 -207 208 -211 212  $ concrete wall #4
205  501 -0.001288 -205 211 -201 202 -203 204  $ concrete wall #5 - pit has opened ceeling
206  588 -2.7 206 -212 -201 202 -203 204  $ concrete wall #6
c    ------
c    Detector volume
c    flight path = front surface of detector
c    detector height = ref UCRL-51144 Fig. 10: 5.7 cm
c    detector diameter is between diameter of PM (15.54 cm) and tube (21.6 cm) - see Fig3 ref UCRL-51144
c    detector diameter was modeled to be 20 cm
c    ------
400  501 -0.001288 -403 -401 402          $ detector volume

c    BEGIN SURFACES:
```

```
1    px  -0.475
2    kx   -16.4914 0.00488998  $ x-cone
3    so   6.0
4    so   10.932
99   so   1500   $ ext boundary
100  p   1 0 0.487733 0    $ source surface
c
c
c      New surfaces for target assembly
c      --------------------------------
c      Taken from Fig. 6 (on page 10) of "Livermore Pulsed Sphere Program:
c      Program Summary Through July 1971", UCRL-51144, Rev I (Feb 10, 1972);
c      also shown as Fig. 2 of Ham Hunter's SINBAD Experiment SBE 17.001 file.
c
c      Note: The vacuum-filled "target assembly" is defined
c      as everything inside the region:  (-101 -111 103)
c      -- ie, everything inside x-cone 101, from x= -0.0775 cm to x=25.9 cm
c
c      In reality, the tritium target (a very thin 1.20-cm-diam cylindrical disk,
c      with R=0.60 cm, from x= -0.0002 cm to x= +0.0002 cm) would lie in the region
c      defined by (-112 -107 106).  In this model, however, we have chosen to NOT
c      explicitly represent this region, but to homogenize the thin tritium disk
c      with the (still pretty thin) 0.001-cm-thick titanium disk containing the
c      tritium disk, and to distribute the neutron source over a 1.20-cm-diam disk
c      on Surf 100 (x=0.0) which specified in the general pulsed sphere model but
c      not explicitly used in this target assembly model.  (That way, this source
c      spec remains valid whether we use this target assembly model or not.)
c
101    kx  -11.9275 0.00476064 $ x-cone of R=0.8231 @ X=0.0005 and R=2.5411 @ X=24.9
102    kx  -11.1883 0.00476064    $ x-cone of R=0.772  @ X=0.0005 and R=2.49   @ X=24.9
103    px -0.0775                      $ xmin for whole "target assembly"
104    px -0.0515          $ plane dividing zones (2=Tungsten) and (3=Alloy) in Fig. 6
105    px -0.0005          $ plane dividing zones (1=Titanium, with trituim) and (2=Tungsten) in Fig. 6
c      106   px -0.0002    $ xmin for the actual tritium source disk
c      107   px 0.0002     $ xmax for the actual tritium source disk
108    px  0.0005          $ plane dividing internal void and zone (1=Titanium) in Fig. 6
109    px  11.9            $ xmin for part-length internal aluminum cylinder
110    px  24.9            $ xmin for back plate of target assembly
111    px  25.9            $ xmax for back plate of target assembly = xmax for whole "target assembly"
c      112    cx 0.60      $ radius of the actual tritium source disk
113    cx  0.63            $ inner radius of part-length internal AL cylinder
114    cx  0.75            $ outer radius of part-length internal AL cylinder
115    px  0.2505          $ plane dividing zones (5=conical AL body) and (4=AL,H,C alloy) in Fig. 6
c      --------------------------------
c
c    ------
c    surfaces for room - concrete pit - 40 ft =12.2 m (UCID-51144), 2m concrete walls
c    in LLNL-PROC-453212 concrete pit modelled with different dimensions (10.24 inner dimension
c    with 2.02 m walls leads to outer dimension of 14.28)
c    reference laur-96-2143 supports model from LLNL-PROC-453212
c    dimensions from LLNL-PROC-453212 were taken as the reference
c    needs to be evaluated as the uncertainty
c    floors are reported to be thick aluminum - unknown thickness, low mass (UICD-17332)
c    taking into account flight path of 746.3 cm for 26deg angle detector is positioned 32.3 cm from the wall
c    ------
201  px 714   $ outer wall 1
202  px -714  $ outer wall 2
203  py 714   $ outer wall 3
204  py -714  $ outer wall 4
205  pz 714   $ outer wall 5
206  pz -550  $ outer wall 6 - floor - thick aluminum
207  px 512   $ inner wall 1 (200 cm thick concrete)
208  px -512  $ inner wall 2 (200 cm thick concrete)
209  py 512   $ inner wall 3 (200 cm thick concrete)
210  py -512  $ inner wall 4 (200 cm thick concrete)
211  pz 512   $ inner wall 5
212  pz -512  $ inner wall 6
c    ------
c    surfaces for 26 deg beamline
c    in reference UCRL-51144 the diameter of Fe tuide through the wall and beyond was reported
c    ID=31.116 cm and OD=32.386 cm
c    colimator modelled as reported in Fig. 3 in UCRL-51144, however it should be noted that
```

```
c    for different spheres different collimators were designed (3 in total) and dimensions of
c    other collimators were not reported, it was only stated that for the low energy measuremnts
c    (at 26deg) the collimation hole was 20-cm hole. Therefore the ID of Fe guide tube was for
c    26deg measurement simulation changed to 20cm, Fe guide tube thicknes remained unchanged.
c    Also other dimensions remained unchanged.
c    ------
301  cx   15.558    $ inner radius of Fe guide tube
302  cx   16.193    $ outer radius of Fe guide tube
303  kx   -840.772 0.000814507 $ first cone for collimator inside wall
304  px   -527.25    $ surface between col1 and col2
305  px   -588.21    $ surface at the end of col2
306  px   -653.62    $ surface at the beginning of col3
307  kx   -787.489 0.00259315 $ second cone for collimator inside wall
308  px   -712.67    $ end of col3 (after col3 is additional Fe and wall dimensions agree with model)
309  cx   3.65       $ final Fe cylindircal hole
c    ------
c    Detector volume
c    in reference UCRL-51144 active detector height is reported to be 5.7 cm
c    from Fig3 it seems detector is covering almost entire inner diameter of Fe guide tube
c    ------
401  px -746.3       $ detector volume surf1
402  px -752         $ detector volume surf2
403  cx  10          $ detector diameter
c    END OF SURFACES (next line must be blank)

c    BEGIN TRANSFORMATIONS:
c    ------
*TR1 0 0 0 26 90 64 90 0 90 116 90 26 1
c    BEGIN PARAMETERS:  (here to end)
c      added random number GEN2 for simulation of runs with higher number of particles
RAND   GEN=2 SEED=15367431640625
mode   n
c       nps     500       $ for quick debug test cases
nps     100000    $ for longer debug test cases
c       nps     1000000   $ for prelim production runs
c       nps     2000000   $ for final  production runs
c       nps    2000000000           $ for extended  production runs
print  -10 -30 -110
c prdmp  j 500000 -1 2
c      cut:n  180.0  0.125  $ ok, gives full coverage(+); measured Tmax < 90 shakes, measured Emin > 0.5 MeV
c      cut:n  180.0  0.125  $ but don't cut here since material may fission
c
imp:n  1 5r 0 1  $ for basic sphere geometry cells (lost particles if imp 0 --> 1)
       1 7r      $ added for target assembly cells
       3 5r      $ importance of the guide tube with colimatiors through wall imp=3
       1 5r      $ importances for concrete pit
       5         $ detector imp=5
c
c
c
c     Marchetti's new source specifications:
c
c     d400 for pulse width is supplied separately
c     since it changes from problem to problem,
c     while everything else stays the same.
c
sdef  pos=0 0 0 dir=d100 erg=fdir=d200 rad=d300 vec=-1 0 0
      sur=100 tme=d400
si100 a  -1.0 -0.9 -0.8 -0.7 -0.6 -0.5 -0.4 -0.3 -0.2 -0.1 0.0
          0.1  0.2  0.3  0.4  0.5  0.6  0.7  0.8  0.9  1.0
sp100     452  454  457  459  461  464  466  469  471  473  476
          478  481  483  485  488  490  493  495  497  500
ds200 q  -1.0  21  -0.9  20  -0.8  19  -0.7  18  -0.6  17
         -0.5  16  -0.4  15  -0.3  14  -0.2  13  -0.1  12
          0.0  11   0.1  10   0.2   9   0.3   8   0.4   7
          0.5   6   0.6   5   0.7   4   0.8   3   0.9   2
          1.0   1
c **** spatial distribution of source ****
si300 h     0 0.6
sp300 d   -21 1
c **** energy distribution ****
si1   a 14.00 14.10 14.20 14.30
```

```
        14.40 14.50 14.60 14.70
        14.80 14.90 15.00 15.10
        15.20 15.30 15.40 15.50
        15.60 15.70 15.80 15.90
sp1      0.0000   0.0000   0.0067   0.2389
         2.2621   8.5730  15.3913  32.3405
        28.8480  27.8023  21.1403  18.0844
        15.4055  12.0301  10.9308   9.2068
         2.4887   0.0000   0.0000   0.0000
si2   a 14.00 14.10 14.20 14.30
        14.40 14.50 14.60 14.70
        14.80 14.90 15.00 15.10
        15.20 15.30 15.40 15.50
sp2      0.0000   0.0000   0.0394   0.5737
         5.0394  13.6361  29.4833  34.1046
        28.6987  24.5471  19.8926  14.8446
        13.9361  11.1899   7.7501   0.0000
si3   a 14.00 14.10 14.20 14.30
        14.40 14.50 14.60 14.70
        14.80 14.90 15.00 15.10
        15.20 15.30 15.40 15.50
sp3      0.0000   0.0000   0.0785   1.7539
         9.2111  23.6081  38.5865  34.3417
        28.0617  21.6143  17.0287  12.9269
        12.2382   3.2725   0.0000   0.0000
si4   a 14.00 14.10 14.20 14.30
        14.40 14.50 14.60 14.70
        14.80 14.90 15.00 15.10
        15.20 15.30 15.40 15.50
sp4      0.0000   0.0000   0.3960   3.9776
        18.2301  40.7022  40.1637  31.6909
        23.2557  17.6923  15.2267  10.3729
         0.0000   0.0000   0.0000   0.0000
si5   a 14.00 14.10 14.20 14.30
        14.40 14.50 14.60 14.70
        14.80 14.90 15.00 15.10
sp5      0.0000   0.0067   1.3001  12.0979
        35.0174  50.8234  35.4343  26.4734
        17.7935  16.0088   5.7390   0.0000
si6   a 14.00 14.10 14.20 14.30
        14.40 14.50 14.60 14.70
        14.80 14.90 15.00 15.10
sp6      0.0000   0.0783   4.2829  30.0627
        56.3041  43.4709  27.8980  21.5204
        16.0633   0.0000   0.0000   0.0000
si7   a 14.00 14.10 14.20 14.30
        14.40 14.50 14.60 14.70
        14.80 14.90 15.00 15.10
sp7      0.0000   0.3948  15.6730  61.0622
        54.0018  33.3282  23.2337  10.9731
         0.0000   0.0000   0.0000   0.0000
si8   a 14.00 14.10 14.20 14.30
        14.40 14.50 14.60 14.70
sp8      0.0000   3.3188  54.4578  70.2145
        39.9746  25.7899   3.8975   0.0000
si9   a 13.60 13.70 13.80 13.90
        14.00 14.10 14.20 14.30
        14.40 14.50 14.60 14.70
sp9      0.0000   0.0000   0.0000   0.0000
         0.0067  26.0337  95.8453  51.5943
        23.1595   0.0000   0.0000   0.0000
si10  a 13.60 13.70 13.80 13.90
        14.00 14.10 14.20 14.30
        14.40 14.50 14.60 14.70
sp10     0.0000   0.0000   0.0000   0.0000
         0.9035 111.2102  68.1255  15.3864
         0.0000   0.0000   0.0000   0.0000
si11  a 13.60 13.70 13.80 13.90
        14.00 14.10 14.20 14.30
sp11     0.0000   0.0000   0.0000   0.0000
        85.1427 106.4852   2.9840   0.0000
si12  a 13.60 13.70 13.80 13.90
```

```
       14.00 14.10 14.20 14.30
sp12    0.0000   0.0000   0.0000   0.0000
        193.5982   0.0000   0.0000   0.0000
si13  a 13.60 13.70 13.80 13.90
       14.00 14.10 14.20 14.30
sp13    0.0000   0.0000   0.0000 192.5454
        0.0391   0.0000   0.0000   0.0000
si14  a 13.60 13.70 13.80 13.90
       14.00 14.10 14.20 14.30
sp14    0.0000   0.0000 165.8002  25.7705
        0.0000   0.0000   0.0000   0.0000
si15  a 13.20 13.30 13.40 13.50
       13.60 13.70 13.80 13.90
       14.00 14.10 14.20 14.30
sp15    0.0000   0.0000   0.0000   0.0000
        16.4808  98.6775  73.5932   1.8055
        0.0000   0.0000   0.0000   0.0000
si16  a 13.20 13.30 13.40 13.50
       13.60 13.70 13.80 13.90
       14.00 14.10 14.20 14.30
sp16    0.0000   0.0000   0.0000  23.7296
       66.2040  83.8084  15.6593   0.1418
        0.0000   0.0000   0.0000   0.0000
si17  a 13.20 13.30 13.40 13.50
       13.60 13.70 13.80 13.90
       14.00 14.10 14.20 14.30
sp17    0.0000   0.0000  27.0418  48.8467
       70.2340  39.1286   3.2608   0.0175
        0.0000   0.0000   0.0000   0.0000
si18  a 12.80 12.90 13.00 13.10
       13.20 13.30 13.40 13.50
       13.60 13.70 13.80 13.90
       14.00 14.10 14.20 14.30
sp18    0.0000   0.0000   0.0000   0.0000
        2.0303  27.2502  37.3878  59.8453
       47.9052  12.2015   0.8937   0.0018
        0.0000   0.0000   0.0000   0.0000
si19  a 12.80 12.90 13.00 13.10
       13.20 13.30 13.40 13.50
       13.60 13.70 13.80 13.90
sp19    0.0000   0.0000   0.0000   6.3499
       22.6144  31.9989  46.6420  49.5506
       25.0656   4.0393   0.2414   0.0000
si20  a 12.80 12.90 13.00 13.10
       13.20 13.30 13.40 13.50
       13.60 13.70 13.80 13.90
sp20    0.0000   0.0000  10.2318  19.7166
       25.7756  38.8741  44.2171  33.6233
       11.2554   1.7554   0.0389   0.0000
si21  a 12.80 12.90 13.00 13.10
       13.20 13.30 13.40 13.50
       13.60 13.70 13.80 13.90
sp21    0.0000  12.6426  16.9782  23.3949
       29.9762  40.9741  38.6652  16.3497
        4.8927   0.5835   0.0174   0.0000
sp400  -41    .200  0    $  FWHM =   .200 shakes =   2.00 ns
c
c
c       BEGIN MATERIAL SPECS
c       ----------------------------------------------------
m501                                  $  Air, nominally at 0.001288 g/cc
        7014.     -0.7885
        8016.     -0.2115
c
m514                                  $  U-238 metal, nominally at 19.04 g/cc
       92238.      0.99
c       6000.      0.005 $ corrected by Denise Neudecker, 3/3/2017 elemental is split into isotopes
        6012.      0.0049465
        6013.      0.0000535
c      14000.      0.005               $ must replace with distribution in ENDF66
       14028.      0.0046115
       14029.      0.0002335
```

```
        14030.      0.0001550
c
m521 $  Concrete, nominally at 2.35 g/cc
c       ------------------
c       Note:  While these 13 "atom fractions" only sum to 0.9966908 (not 1.000000),
c       they were taken from page 142 of LA-12885 (Dec 1994).  Moreover, the atom
c       fractions for the first 8 entries (O, H, Si, Ca, Al, C, Mg, and Na) are also
c       the same as given on pp 309 & 315 of UCRL-51144, Rev I (Feb 1972), which goes
c       on to simply note that the trace elements Fe, K (missing here), Ti, and Mn
c       each account for less than 1.0 at% (each).  While one could speculate that
c       potassium (K=19000) might account for the missing 0.33092 at% (at frac=
c       0.0033092), or that the LANL numbers for the trace elements (last 5 entries)
c       should be renormalized to sum to 1.3 at% (at frac=0.013), such small changes
c       would be well below the uncertainties in most composition specs. In the absence
c       of any clear knowledge on this negligible quantity, we have chosen to simply
c       keep the same traditional material specs previously used by LANL in LA-12885.
c       In this case, mcnp will automatically adjust all fractions to sum to 1.0 exactly.
c       ------------------
         8016.      0.557
         1001.      0.151
c       14000.      0.149               $ must replace with distribution in ENDF66
        14028.      0.1374227
        14029.      0.0069583
        14030.      0.0046190
c       20000.      0.036 $ corrected by Denise Neudecker, 3/3/2017 elemental is split into isotopes
        20040.      0.034899
        20042.      0.000239
        20043.      0.000049
        20044.      0.000751
        20046.      0.000001
        20048.      0.000067
        13027.      0.032
c        6000.      0.031 $ corrected by Denise Neudecker, 3/3/2017 elemental is split into isotopes
         6012.      0.03067
         6013.      0.00033
c       12000.      0.018  $ corrected by Denise Neudecker, 3/3/2017 elemental is split into isotopes
        12024.      0.014218
        12025.      0.001800
        12026.      0.001982
        11023.      0.013
        26054.      0.0001914
        26056.      0.0030268
        26057.      0.0000726
c       22000.      0.0033 $ corrected by Denise Neudecker, 3/3/2017 elemental is split into isotopes
        22046.      0.0002723
        22047.      0.0002455
        22048.      0.0024328
        22049.      0.0001785
        22050.      0.0001709
        25055.      0.0031
c
m581 $  Target Material (50 at% Tritium, 50 at% Titanium), nominally at 1.879497 g/cc
c       ------------------
c       Note:  This thin foil (see zone 1 of Fig 6 on page 10 of UCRL-51144)
c       actually has a known mass of only 0.004 grams !!
c       ------------------
         1003.      0.5
c       22000.      0.5 $  corrected by Denise Neudecker, 3/3/2017 elemental is split into isotopes
        22046.      0.041250
        22047.      0.037200
        22048.      0.368600
        22049.      0.027050
        22050.      0.025900
c
m582 $  Target Component (all Tungsten), artificially at 30.073815 g/cc in model
c       ------------------
c       Note:  The larger-than-normal density (indicated here but actually specified
c       on the mcnp cell card) is such that it will exactly replicate the known mass
c       (3.250 grams) of zone 2 in Fig 6 when used in combination with the mcnp model
c       which exactly replicates the geometry in Fig 6. This larger-than-normal density
c       stems from the fact that Fig 6 on page 10 of UCRL-51144 is an "idealized"
c       representation of the target assembly while the stated masses were measured.
```

```
c       ------------------
        74182.      0.2643
        74183.      0.143
        74184.      0.3067
        74186.      0.286
c
m583 $  Target Component (mostly Iron and Copper), artificially at 20.096000 g/cc in model
c       ------------------
c       Note 1:  The "atom fractions" used here sum to 1.06 which cannot be right.
c       Yet, they are "exactly" the same atom fractions given for zone 3 of the
c       target assembly in Fig 6 on page 10 of UCRL-51144, Rev I (Feb 1972).  In
c       the absence of any new (corrected) information, the best we can do is to
c       stay with the original specs and let mcnp automatically renormalize each
c       one so they sum to 1.000 exactly.
c       Note 2:  The larger-than-normal density (indicated here but actually specified
c       on the mcnp cell card) is such that it will exactly replicate the known mass
c       (1.100 grams) of zone 3 in Fig 6 when used in combination with the mcnp model
c       which exactly replicates the geometry in Fig 6. This larger-than-normal density
c       stems from the fact that Fig 6 on page 10 of UCRL-51144 is an "idealized"
c       representation of the target assembly while the stated masses were measured.
c       ------------------
        26054.      0.0261
        26056.      0.4127
        26057.      0.0099
        26058.      0.0013
        29063.      0.2213
        29065.      0.0987
         1001.      0.13
         8016.      0.08
        13027.      0.02
c        6000.      0.06 $  corrected by Denise Neudecker, 3/3/2017 elemental is split into isotopes
        6012.      0.05936
        6013.      0.00064
c
m584 $  Target Component (AL, H, and C) artificially at 23.180464 g/cc in model
c       ------------------
c       Note:  The larger-than-normal density (indicated here but actually specified
c       on the mcnp cell card) is such that it will exactly replicate the known mass
c       (1.500 grams) of zone 4 in Fig 6 when used in combination with the mcnp model
c       which exactly replicates the geometry in Fig 6. This larger-than-normal density
c       stems from the fact that Fig 6 on page 10 of UCRL-51144 is an "idealized"
c       representation of the target assembly while the stated masses were measured.
c       ------------------
        13027.      0.5
         1001.      0.30
c        6000.      0.20 $  corrected by Denise Neudecker, 3/3/2017 elemental is split into isotopes
         6012.      0.19786
         6013.      0.00214
c
m585 $  Target Component (all Aluminum), nominally at 2.701353 g/cc in model
        13027.      1.0
c
m586 $  Target Component (all Aluminum), nominally at 2.705809 g/cc in model
        13027.      1.0
c
m587 $  Target Component (Aluminum and Copper) artificially at 20.008000 g/cc in model
c       ------------------
c       Note:  The larger-than-normal density (indicated here but actually specified
c       on the mcnp cell card) is such that it will exactly replicate the known mass
c       (417.000 grams) of zone 7 in Fig 6 when used in combination with the mcnp model
c       which exactly replicates the geometry in Fig 6. This larger-than-normal density
c       stems from the fact that Fig 6 on page 10 of UCRL-51144 is an "idealized"
c       representation of the target assembly while the stated masses were measured.
c       ------------------
        13027.      0.5
        29063.      0.3459
        29065.      0.1541
c       ------------------------------------------------------
m588  $ Aluminum floor, unknown density, assumed: 2.7 g/cc
        13027.     1.0
m589  $ Iron for colimator, unknown impurities or isotopic composition, asumed natural
        26054.     6.3031E-4
```

```
        26056.     9.8944E-3
        26057.     2.2851E-4
        26058.     3.0410E-5
m590  $ Borated Paraffin (atomic fractions reported in UCRL 51144)
c     density was not reported, chosen 1.35 g/cc (matweb HDPE - 18% borated polyethilen)
         6012.     2.8690E-1
         6013.     3.1030E-3
         1001.     5.8000E-1
         5010.     2.5870E-2
         5011.     1.0413E-1
c       END OF MATERIAL SPECS
c
c
c    ********************************************************************************
c    BEGIN DETECTOR TALLY SPECIFICATIONS
c
c
c    If fwhm = 0.2 shakes = 2 ns, then ....
c    ---------------------------------
fc204 28u2.8b(T):  NE213-B (Bias=1.6) Det Resp vs T, Path=746.34 cm, 26 deg line
f204:n 400 $ tally inside detector volume
c
c     NE213B (Bias=1.6 MeV) Detector Response Function used
c     in the 30-deg and 120-deg Beamlines, from UCID-17332
c     Note: this uses lin-lin interp, not the default log-log.
c
de204 lin 1.60     1.80     1.90     2.00     2.10     2.20     2.30     2.40
          2.50     2.75     3.00     3.50     4.00     4.50     5.00     5.50
          6.00     6.40     6.60     6.80     7.00     7.50     8.10     8.50
          9.00    10.00    11.00    12.00    12.50    13.00    13.50    14.00
         15.00    16.00
c
df204 lin $ same NE213B (Bias=1.6 MeV) data, renormalized to 1.0 at 15.0 MeV:
        0.0000   0.4740   0.6039   0.7338   0.8377   0.9740   1.0682   1.1104
        1.1786   1.2825   1.3312   1.3799   1.4058   1.4253   1.4286   1.4188
        1.3896   1.3474   1.3636   1.3571   1.3377   1.2890   1.2338   1.2240
        1.1851   1.1169   1.0519   0.9935   0.9773   0.9675   0.9675   0.9773
        1.0000   1.0552
c       end of NE213B (Bias=1.6 MeV) data
c
c    Note:  the "time points" given in the experimental data were actually the
c    times at the midpoints of the experimental time bins, with the reported
c    count rates being the integral over the experiental time bins.  Here we
c    have used the reported "time points" to recreate the original "time bins".
c
t204  $ time bins in shakes (not nanoseconds)
        1.28000E+01  1.30000E+01  1.32000E+01  1.34000E+01  1.36000E+01
        1.38000E+01  1.40000E+01  1.42000E+01  1.44000E+01  1.46000E+01
        1.48000E+01  1.50000E+01  1.52000E+01  1.54000E+01  1.56000E+01
        1.58000E+01  1.60000E+01  1.62000E+01  1.64000E+01  1.66000E+01
        1.68000E+01  1.70000E+01  1.72000E+01  1.74000E+01  1.76000E+01
        1.78000E+01  1.80000E+01  1.82000E+01  1.84000E+01  1.86000E+01
        1.88000E+01  1.90000E+01  1.92000E+01  1.94000E+01  1.96000E+01
        1.98000E+01  2.00000E+01  2.02000E+01  2.04000E+01  2.06000E+01
        2.08000E+01  2.10000E+01  2.12000E+01  2.14000E+01  2.16000E+01
        2.18000E+01  2.20000E+01  2.22000E+01  2.24000E+01  2.26000E+01
        2.28000E+01  2.30000E+01  2.32000E+01  2.34000E+01  2.36000E+01
        2.38000E+01  2.40000E+01  2.42000E+01  2.44000E+01  2.46000E+01
        2.48000E+01  2.50000E+01  2.52000E+01  2.54000E+01  2.56000E+01
        2.58000E+01  2.60000E+01  2.62000E+01  2.64000E+01  2.66000E+01
        2.68000E+01  2.70000E+01  2.72000E+01  2.74000E+01  2.76000E+01
        2.78000E+01  2.80000E+01  2.82000E+01  2.84000E+01  2.86000E+01
        2.88000E+01  2.90000E+01  2.92000E+01  2.94000E+01  2.96000E+01
        2.98000E+01  3.00000E+01  3.02000E+01  3.04000E+01  3.06000E+01
        3.08000E+01  3.10000E+01  3.12000E+01  3.14000E+01  3.16000E+01
        3.18000E+01  3.20000E+01  3.22000E+01  3.24000E+01  3.26000E+01
        3.28000E+01  3.30000E+01  3.32000E+01  3.34000E+01  3.36000E+01
        3.38000E+01  3.40000E+01  3.42000E+01  3.44000E+01  3.46000E+01
        3.48000E+01  3.50000E+01  3.52000E+01  3.54000E+01  3.56000E+01
        3.58000E+01  3.60000E+01  3.62000E+01  3.64000E+01  3.66000E+01
        3.68000E+01  3.70000E+01  3.72000E+01  3.74000E+01  3.76000E+01
        3.78000E+01  3.80000E+01  3.82000E+01  3.84000E+01  3.86000E+01
```

```
        3.88000E+01  3.90000E+01  3.92000E+01  3.94000E+01  3.96000E+01
        3.98000E+01  4.00000E+01  4.02000E+01  4.04000E+01
fq204  f  d  u  s  m  c  t  e   $ new hierarchy puts time in vertical column
c
c
fc214 28u2.8b(E):  NE213-B (Bias=1.6) Det Resp vs E, Path=746.34 cm, 26 deg line
f214:n 400 $ tally inside detector volume
c
c     NE213B (Bias=1.6 MeV) Detector Response Function used
c     in the 30-deg and 120-deg Beamlines, from UCID-17332
c     Note: this uses lin-lin interp, not the default log-log.
c
de214 lin 1.60     1.80     1.90     2.00     2.10     2.20     2.30     2.40
          2.50     2.75     3.00     3.50     4.00     4.50     5.00     5.50
          6.00     6.40     6.60     6.80     7.00     7.50     8.10     8.50
          9.00    10.00    11.00    12.00    12.50    13.00    13.50    14.00
         15.00    16.00
c
df214 lin $ same NE213B (Bias=1.6 MeV) data, renormalized to 1.0 at 15.0 MeV:
        0.0000   0.4740   0.6039   0.7338   0.8377   0.9740   1.0682   1.1104
        1.1786   1.2825   1.3312   1.3799   1.4058   1.4253   1.4286   1.4188
        1.3896   1.3474   1.3636   1.3571   1.3377   1.2890   1.2338   1.2240
        1.1851   1.1169   1.0519   0.9935   0.9773   0.9675   0.9675   0.9773
        1.0000   1.0552
c       end of NE213B (Bias=1.6 MeV) data
c
c    Note:  The original experimental count rates were gathered in time bins, not
c    energy bins (and certainly not at energy points).  [Thus, the most meaningful
c    comparisons of calculations to experiments should be made based on the time bins,
c    not the energy bins.]  Still, there is some limited interest in the energy bins.
c    The "energy points" given in the experimental data listings were actually based
c    on a relativistic "first-flight" energy vs flight time relationship in which
c       E= rme*((1.0/dsqrt(1.0-(fp*fp/(t*t*c*c))))-1.0)
c    where
c       c= velocity of light = 29.97925 cm/nanosecond
c       t= the time (in nanoseconds), at the midpoint of the time bin
c       fp= the length of the flightpath (in cm)
c       rme= the rest mass energy of a neutron (939.550 MeV)
c       E= the energy of the neutron
c    For the "energy bins" used in MCNP, the "energy bin boundaries" (based on this
c    same relationship) are determined by the more well-known "time bin boundaries".
c
e214  $ energy bins in MeV
        1.78907E+00  1.80697E+00  1.82512E+00  1.84356E+00
        1.86231E+00  1.88131E+00  1.90061E+00  1.92021E+00  1.94011E+00
        1.96036E+00  1.98091E+00  2.00176E+00  2.02296E+00  2.04451E+00
        2.06636E+00  2.08860E+00  2.11120E+00  2.13415E+00  2.15750E+00
        2.18120E+00  2.20535E+00  2.22990E+00  2.25480E+00  2.28015E+00
        2.30594E+00  2.33219E+00  2.35889E+00  2.38599E+00  2.41359E+00
        2.44169E+00  2.47029E+00  2.49939E+00  2.52898E+00  2.55913E+00
        2.58978E+00  2.62103E+00  2.65288E+00  2.68528E+00  2.71827E+00
        2.75187E+00  2.78607E+00  2.82092E+00  2.85647E+00  2.89266E+00
        2.92956E+00  2.96721E+00  3.00556E+00  3.04465E+00  3.08450E+00
        3.12515E+00  3.16665E+00  3.20894E+00  3.25209E+00  3.29614E+00
        3.34103E+00  3.38688E+00  3.43373E+00  3.48152E+00  3.53032E+00
        3.58012E+00  3.63101E+00  3.68301E+00  3.73610E+00  3.79040E+00
        3.84590E+00  3.90259E+00  3.96054E+00  4.01978E+00  4.08038E+00
        4.14237E+00  4.20582E+00  4.27076E+00  4.33715E+00  4.40510E+00
        4.47469E+00  4.54598E+00  4.61898E+00  4.69372E+00  4.77031E+00
        4.84880E+00  4.92925E+00  5.01169E+00  5.09628E+00  5.18302E+00
        5.27196E+00  5.36325E+00  5.45694E+00  5.55308E+00  5.65182E+00
        5.75321E+00  5.85734E+00  5.96438E+00  6.07437E+00  6.18745E+00
        6.30374E+00  6.42332E+00  6.54635E+00  6.67298E+00  6.80337E+00
        6.93760E+00  7.07583E+00  7.21826E+00  7.36503E+00  7.51636E+00
        7.67243E+00  7.83346E+00  7.99963E+00  8.17115E+00  8.34827E+00
        8.53124E+00  8.72030E+00  8.91572E+00  9.11783E+00  9.32699E+00
        9.54344E+00  9.76755E+00  9.99975E+00  1.02404E+01  1.04898E+01
        1.07483E+01  1.10167E+01  1.12957E+01  1.15851E+01  1.18855E+01
        1.21979E+01  1.25233E+01  1.28622E+01  1.32147E+01  1.35820E+01
        1.39654E+01  1.43648E+01  1.47817E+01  1.52175E+01  1.56734E+01
        1.61497E+01  1.66480E+01  1.71703E+01  1.77181E+01  1.82927E+01
fq214  f  d  u  s  m  c  e  t   $ std hierarchy puts energy in vertical column
```

```
c    If fwhm = 0.2 shakes = 2 ns, then ....
c    --------------------------------
fc202 28u2.8b(T):  NE213-B (Bias=1.6) Det Resp vs T, Path=746.34 cm, 26 deg line
f202:n 401 $ tally ifront detector surface
c
c     NE213B (Bias=1.6 MeV) Detector Response Function used
c     in the 30-deg and 120-deg Beamlines, from UCID-17332
c     Note: this uses lin-lin interp, not the default log-log.
c
de202 lin 1.60     1.80     1.90     2.00     2.10     2.20     2.30     2.40
          2.50     2.75     3.00     3.50     4.00     4.50     5.00     5.50
          6.00     6.40     6.60     6.80     7.00     7.50     8.10     8.50
          9.00    10.00    11.00    12.00    12.50    13.00    13.50    14.00
         15.00    16.00
c
df202 lin $ same NE213B (Bias=1.6 MeV) data, renormalized to 1.0 at 15.0 MeV:
        0.0000   0.4740   0.6039   0.7338   0.8377   0.9740   1.0682   1.1104
        1.1786   1.2825   1.3312   1.3799   1.4058   1.4253   1.4286   1.4188
        1.3896   1.3474   1.3636   1.3571   1.3377   1.2890   1.2338   1.2240
        1.1851   1.1169   1.0519   0.9935   0.9773   0.9675   0.9675   0.9773
        1.0000   1.0552
c       end of NE213B (Bias=1.6 MeV) data
c
c    Note:  the "time points" given in the experimental data were actually the
c    times at the midpoints of the experimental time bins, with the reported
c    count rates being the integral over the experiental time bins.  Here we
c    have used the reported "time points" to recreate the original "time bins".
c
t202  $ time bins in shakes (not nanoseconds)
        1.28000E+01  1.30000E+01  1.32000E+01  1.34000E+01  1.36000E+01
        1.38000E+01  1.40000E+01  1.42000E+01  1.44000E+01  1.46000E+01
        1.48000E+01  1.50000E+01  1.52000E+01  1.54000E+01  1.56000E+01
        1.58000E+01  1.60000E+01  1.62000E+01  1.64000E+01  1.66000E+01
        1.68000E+01  1.70000E+01  1.72000E+01  1.74000E+01  1.76000E+01
        1.78000E+01  1.80000E+01  1.82000E+01  1.84000E+01  1.86000E+01
        1.88000E+01  1.90000E+01  1.92000E+01  1.94000E+01  1.96000E+01
        1.98000E+01  2.00000E+01  2.02000E+01  2.04000E+01  2.06000E+01
        2.08000E+01  2.10000E+01  2.12000E+01  2.14000E+01  2.16000E+01
        2.18000E+01  2.20000E+01  2.22000E+01  2.24000E+01  2.26000E+01
        2.28000E+01  2.30000E+01  2.32000E+01  2.34000E+01  2.36000E+01
        2.38000E+01  2.40000E+01  2.42000E+01  2.44000E+01  2.46000E+01
        2.48000E+01  2.50000E+01  2.52000E+01  2.54000E+01  2.56000E+01
        2.58000E+01  2.60000E+01  2.62000E+01  2.64000E+01  2.66000E+01
        2.68000E+01  2.70000E+01  2.72000E+01  2.74000E+01  2.76000E+01
        2.78000E+01  2.80000E+01  2.82000E+01  2.84000E+01  2.86000E+01
        2.88000E+01  2.90000E+01  2.92000E+01  2.94000E+01  2.96000E+01
        2.98000E+01  3.00000E+01  3.02000E+01  3.04000E+01  3.06000E+01
        3.08000E+01  3.10000E+01  3.12000E+01  3.14000E+01  3.16000E+01
        3.18000E+01  3.20000E+01  3.22000E+01  3.24000E+01  3.26000E+01
        3.28000E+01  3.30000E+01  3.32000E+01  3.34000E+01  3.36000E+01
        3.38000E+01  3.40000E+01  3.42000E+01  3.44000E+01  3.46000E+01
        3.48000E+01  3.50000E+01  3.52000E+01  3.54000E+01  3.56000E+01
        3.58000E+01  3.60000E+01  3.62000E+01  3.64000E+01  3.66000E+01
        3.68000E+01  3.70000E+01  3.72000E+01  3.74000E+01  3.76000E+01
        3.78000E+01  3.80000E+01  3.82000E+01  3.84000E+01  3.86000E+01
        3.88000E+01  3.90000E+01  3.92000E+01  3.94000E+01  3.96000E+01
        3.98000E+01  4.00000E+01  4.02000E+01  4.04000E+01
fq202  f  d  u  s  m  c  t  e   $ new hierarchy puts time in vertical column
c
c
fc212 28u2.8b(E):  NE213-B (Bias=1.6) Det Resp vs E, Path=746.34 cm, 26 deg line
f212:n 401 $ tally front detector surface
c
c     NE213B (Bias=1.6 MeV) Detector Response Function used
c     in the 30-deg and 120-deg Beamlines, from UCID-17332
c     Note: this uses lin-lin interp, not the default log-log.
c
de212 lin 1.60     1.80     1.90     2.00     2.10     2.20     2.30     2.40
          2.50     2.75     3.00     3.50     4.00     4.50     5.00     5.50
          6.00     6.40     6.60     6.80     7.00     7.50     8.10     8.50
          9.00    10.00    11.00    12.00    12.50    13.00    13.50    14.00
         15.00    16.00
```

```
c
df212 lin $ same NE213B (Bias=1.6 MeV) data, renormalized to 1.0 at 15.0 MeV:
        0.0000   0.4740   0.6039   0.7338   0.8377   0.9740   1.0682   1.1104
        1.1786   1.2825   1.3312   1.3799   1.4058   1.4253   1.4286   1.4188
        1.3896   1.3474   1.3636   1.3571   1.3377   1.2890   1.2338   1.2240
        1.1851   1.1169   1.0519   0.9935   0.9773   0.9675   0.9675   0.9773
        1.0000   1.0552
c       end of NE213B (Bias=1.6 MeV) data
c
c    Note:  The original experimental count rates were gathered in time bins, not
c    energy bins (and certainly not at energy points).  [Thus, the most meaningful
c    comparisons of calculations to experiments should be made based on the time bins,
c    not the energy bins.]  Still, there is some limited interest in the energy bins.
c    The "energy points" given in the experimental data listings were actually based
c    on a relativistic "first-flight" energy vs flight time relationship in which
c       E= rme*((1.0/dsqrt(1.0-(fp*fp/(t*t*c*c))))-1.0)
c    where
c       c= velocity of light = 29.97925 cm/nanosecond
c       t= the time (in nanoseconds), at the midpoint of the time bin
c       fp= the length of the flightpath (in cm)
c       rme= the rest mass energy of a neutron (939.550 MeV)
c       E= the energy of the neutron
c    For the "energy bins" used in MCNP, the "energy bin boundaries" (based on this
c    same relationship) are determined by the more well-known "time bin boundaries".
c
e212  $ energy bins in MeV
        1.78907E+00  1.80697E+00  1.82512E+00  1.84356E+00
        1.86231E+00  1.88131E+00  1.90061E+00  1.92021E+00  1.94011E+00
        1.96036E+00  1.98091E+00  2.00176E+00  2.02296E+00  2.04451E+00
        2.06636E+00  2.08860E+00  2.11120E+00  2.13415E+00  2.15750E+00
        2.18120E+00  2.20535E+00  2.22990E+00  2.25480E+00  2.28015E+00
        2.30594E+00  2.33219E+00  2.35889E+00  2.38599E+00  2.41359E+00
        2.44169E+00  2.47029E+00  2.49939E+00  2.52898E+00  2.55913E+00
        2.58978E+00  2.62103E+00  2.65288E+00  2.68528E+00  2.71827E+00
        2.75187E+00  2.78607E+00  2.82092E+00  2.85647E+00  2.89266E+00
        2.92956E+00  2.96721E+00  3.00556E+00  3.04465E+00  3.08450E+00
        3.12515E+00  3.16665E+00  3.20894E+00  3.25209E+00  3.29614E+00
        3.34103E+00  3.38688E+00  3.43373E+00  3.48152E+00  3.53032E+00
        3.58012E+00  3.63101E+00  3.68301E+00  3.73610E+00  3.79040E+00
        3.84590E+00  3.90259E+00  3.96054E+00  4.01978E+00  4.08038E+00
        4.14237E+00  4.20582E+00  4.27076E+00  4.33715E+00  4.40510E+00
        4.47469E+00  4.54598E+00  4.61898E+00  4.69372E+00  4.77031E+00
        4.84880E+00  4.92925E+00  5.01169E+00  5.09628E+00  5.18302E+00
        5.27196E+00  5.36325E+00  5.45694E+00  5.55308E+00  5.65182E+00
        5.75321E+00  5.85734E+00  5.96438E+00  6.07437E+00  6.18745E+00
        6.30374E+00  6.42332E+00  6.54635E+00  6.67298E+00  6.80337E+00
        6.93760E+00  7.07583E+00  7.21826E+00  7.36503E+00  7.51636E+00
        7.67243E+00  7.83346E+00  7.99963E+00  8.17115E+00  8.34827E+00
        8.53124E+00  8.72030E+00  8.91572E+00  9.11783E+00  9.32699E+00
        9.54344E+00  9.76755E+00  9.99975E+00  1.02404E+01  1.04898E+01
        1.07483E+01  1.10167E+01  1.12957E+01  1.15851E+01  1.18855E+01
        1.21979E+01  1.25233E+01  1.28622E+01  1.32147E+01  1.35820E+01
        1.39654E+01  1.43648E+01  1.47817E+01  1.52175E+01  1.56734E+01
        1.61497E+01  1.66480E+01  1.71703E+01  1.77181E+01  1.82927E+01
fq212  f  d  u  s  m  c  e  t   $ std hierarchy puts energy in vertical column
c    ---------------------------------
fc205 28u2.8b(T):  NE213-B (Bias=1.6) Det Resp vs T, Path=746.34 cm, 26 deg line
f205:n      -746.34 0 0 0 $ point detector tally
c
c     NE213B (Bias=1.6 MeV) Detector Response Function used
c     in the 30-deg and 120-deg Beamlines, from UCID-17332
c     Note: this uses lin-lin interp, not the default log-log.
c
de205 lin 1.60     1.80     1.90     2.00     2.10     2.20     2.30     2.40
          2.50     2.75     3.00     3.50     4.00     4.50     5.00     5.50
          6.00     6.40     6.60     6.80     7.00     7.50     8.10     8.50
          9.00    10.00    11.00    12.00    12.50    13.00    13.50    14.00
         15.00    16.00
c
df205 lin $ same NE213B (Bias=1.6 MeV) data, renormalized to 1.0 at 15.0 MeV:
        0.0000   0.4740   0.6039   0.7338   0.8377   0.9740   1.0682   1.1104
        1.1786   1.2825   1.3312   1.3799   1.4058   1.4253   1.4286   1.4188
```

```
        1.3896   1.3474   1.3636   1.3571   1.3377   1.2890   1.2338   1.2240
        1.1851   1.1169   1.0519   0.9935   0.9773   0.9675   0.9675   0.9773
        1.0000   1.0552
c       end of NE213B (Bias=1.6 MeV) data
c
c    Note:  the "time points" given in the experimental data were actually the
c    times at the midpoints of the experimental time bins, with the reported
c    count rates being the integral over the experiental time bins.  Here we
c    have used the reported "time points" to recreate the original "time bins".
c
t205  $ time bins in shakes (not nanoseconds)
        1.28000E+01  1.30000E+01  1.32000E+01  1.34000E+01  1.36000E+01
        1.38000E+01  1.40000E+01  1.42000E+01  1.44000E+01  1.46000E+01
        1.48000E+01  1.50000E+01  1.52000E+01  1.54000E+01  1.56000E+01
        1.58000E+01  1.60000E+01  1.62000E+01  1.64000E+01  1.66000E+01
        1.68000E+01  1.70000E+01  1.72000E+01  1.74000E+01  1.76000E+01
        1.78000E+01  1.80000E+01  1.82000E+01  1.84000E+01  1.86000E+01
        1.88000E+01  1.90000E+01  1.92000E+01  1.94000E+01  1.96000E+01
        1.98000E+01  2.00000E+01  2.02000E+01  2.04000E+01  2.06000E+01
        2.08000E+01  2.10000E+01  2.12000E+01  2.14000E+01  2.16000E+01
        2.18000E+01  2.20000E+01  2.22000E+01  2.24000E+01  2.26000E+01
        2.28000E+01  2.30000E+01  2.32000E+01  2.34000E+01  2.36000E+01
        2.38000E+01  2.40000E+01  2.42000E+01  2.44000E+01  2.46000E+01
        2.48000E+01  2.50000E+01  2.52000E+01  2.54000E+01  2.56000E+01
        2.58000E+01  2.60000E+01  2.62000E+01  2.64000E+01  2.66000E+01
        2.68000E+01  2.70000E+01  2.72000E+01  2.74000E+01  2.76000E+01
        2.78000E+01  2.80000E+01  2.82000E+01  2.84000E+01  2.86000E+01
        2.88000E+01  2.90000E+01  2.92000E+01  2.94000E+01  2.96000E+01
        2.98000E+01  3.00000E+01  3.02000E+01  3.04000E+01  3.06000E+01
        3.08000E+01  3.10000E+01  3.12000E+01  3.14000E+01  3.16000E+01
        3.18000E+01  3.20000E+01  3.22000E+01  3.24000E+01  3.26000E+01
        3.28000E+01  3.30000E+01  3.32000E+01  3.34000E+01  3.36000E+01
        3.38000E+01  3.40000E+01  3.42000E+01  3.44000E+01  3.46000E+01
        3.48000E+01  3.50000E+01  3.52000E+01  3.54000E+01  3.56000E+01
        3.58000E+01  3.60000E+01  3.62000E+01  3.64000E+01  3.66000E+01
        3.68000E+01  3.70000E+01  3.72000E+01  3.74000E+01  3.76000E+01
        3.78000E+01  3.80000E+01  3.82000E+01  3.84000E+01  3.86000E+01
        3.88000E+01  3.90000E+01  3.92000E+01  3.94000E+01  3.96000E+01
        3.98000E+01  4.00000E+01  4.02000E+01  4.04000E+01
fq205  f  d  u  s  m  c  t  e   $ new hierarchy puts time in vertical column
c
c
fc215 28u2.8b(E):  NE213-B (Bias=1.6) Det Resp vs E, Path=746.34 cm, 26 deg line
f215:n      -746.34 0 0 0 $ point detector tally
c
c     NE213B (Bias=1.6 MeV) Detector Response Function used
c     in the 30-deg and 120-deg Beamlines, from UCID-17332
c     Note: this uses lin-lin interp, not the default log-log.
c
de215 lin 1.60     1.80     1.90     2.00     2.10     2.20     2.30     2.40
          2.50     2.75     3.00     3.50     4.00     4.50     5.00     5.50
          6.00     6.40     6.60     6.80     7.00     7.50     8.10     8.50
          9.00    10.00    11.00    12.00    12.50    13.00    13.50    14.00
         15.00    16.00
c
df215 lin $ same NE213B (Bias=1.6 MeV) data, renormalized to 1.0 at 15.0 MeV:
        0.0000   0.4740   0.6039   0.7338   0.8377   0.9740   1.0682   1.1104
        1.1786   1.2825   1.3312   1.3799   1.4058   1.4253   1.4286   1.4188
        1.3896   1.3474   1.3636   1.3571   1.3377   1.2890   1.2338   1.2240
        1.1851   1.1169   1.0519   0.9935   0.9773   0.9675   0.9675   0.9773
        1.0000   1.0552
c       end of NE213B (Bias=1.6 MeV) data
c
c    Note:  The original experimental count rates were gathered in time bins, not
c    energy bins (and certainly not at energy points).  [Thus, the most meaningful
c    comparisons of calculations to experiments should be made based on the time bins,
c    not the energy bins.]  Still, there is some limited interest in the energy bins.
c    The "energy points" given in the experimental data listings were actually based
c    on a relativistic "first-flight" energy vs flight time relationship in which
c       E= rme*((1.0/dsqrt(1.0-(fp*fp/(t*t*c*c))))-1.0)
c    where
c       c= velocity of light = 29.97925 cm/nanosecond
```

```
c       t= the time (in nanoseconds), at the midpoint of the time bin
c       fp= the length of the flightpath (in cm)
c       rme= the rest mass energy of a neutron (939.550 MeV)
c       E= the energy of the neutron
c    For the "energy bins" used in MCNP, the "energy bin boundaries" (based on this
c    same relationship) are determined by the more well-known "time bin boundaries".
c
e215  $ energy bins in MeV
        1.78907E+00  1.80697E+00  1.82512E+00  1.84356E+00
        1.86231E+00  1.88131E+00  1.90061E+00  1.92021E+00  1.94011E+00
        1.96036E+00  1.98091E+00  2.00176E+00  2.02296E+00  2.04451E+00
        2.06636E+00  2.08860E+00  2.11120E+00  2.13415E+00  2.15750E+00
        2.18120E+00  2.20535E+00  2.22990E+00  2.25480E+00  2.28015E+00
        2.30594E+00  2.33219E+00  2.35889E+00  2.38599E+00  2.41359E+00
        2.44169E+00  2.47029E+00  2.49939E+00  2.52898E+00  2.55913E+00
        2.58978E+00  2.62103E+00  2.65288E+00  2.68528E+00  2.71827E+00
        2.75187E+00  2.78607E+00  2.82092E+00  2.85647E+00  2.89266E+00
        2.92956E+00  2.96721E+00  3.00556E+00  3.04465E+00  3.08450E+00
        3.12515E+00  3.16665E+00  3.20894E+00  3.25209E+00  3.29614E+00
        3.34103E+00  3.38688E+00  3.43373E+00  3.48152E+00  3.53032E+00
        3.58012E+00  3.63101E+00  3.68301E+00  3.73610E+00  3.79040E+00
        3.84590E+00  3.90259E+00  3.96054E+00  4.01978E+00  4.08038E+00
        4.14237E+00  4.20582E+00  4.27076E+00  4.33715E+00  4.40510E+00
        4.47469E+00  4.54598E+00  4.61898E+00  4.69372E+00  4.77031E+00
        4.84880E+00  4.92925E+00  5.01169E+00  5.09628E+00  5.18302E+00
        5.27196E+00  5.36325E+00  5.45694E+00  5.55308E+00  5.65182E+00
        5.75321E+00  5.85734E+00  5.96438E+00  6.07437E+00  6.18745E+00
        6.30374E+00  6.42332E+00  6.54635E+00  6.67298E+00  6.80337E+00
        6.93760E+00  7.07583E+00  7.21826E+00  7.36503E+00  7.51636E+00
        7.67243E+00  7.83346E+00  7.99963E+00  8.17115E+00  8.34827E+00
        8.53124E+00  8.72030E+00  8.91572E+00  9.11783E+00  9.32699E+00
        9.54344E+00  9.76755E+00  9.99975E+00  1.02404E+01  1.04898E+01
        1.07483E+01  1.10167E+01  1.12957E+01  1.15851E+01  1.18855E+01
        1.21979E+01  1.25233E+01  1.28622E+01  1.32147E+01  1.35820E+01
        1.39654E+01  1.43648E+01  1.47817E+01  1.52175E+01  1.56734E+01
        1.61497E+01  1.66480E+01  1.71703E+01  1.77181E+01  1.82927E+01
fq215  f  d  u  s  m  c  e  t   $ std hierarchy puts energy in vertical column
c
c
c    END OF ALL DATA (next 2 lines must be blank)
```

Nuclear Data Section
International Atomic Energy Agency
Vienna International Centre, P.O. Box 100
A-1400 Vienna, Austria

E-mail: nds.contact-point@iaea.org
Fax: (43-1) 26007
Telephone: (43-1) 2600 21725
Web: http://www-nds.iaea.org